AD_____

Award Number: W81XWH-04-1-0149

TITLE: The Role of the Caspase-8 Inhibitor FLIP in Androgen-Withdrawal Induced Death of Prostate Epithelium

PRINCIPAL INVESTIGATOR: John Krolewski, MD-PhD
Kent Nastiuk, PhD

CONTRACTING ORGANIZATION: University of California
Irvine CA 92679-7600

REPORT DATE: January 2007

TYPE OF REPORT: Final

PREPARED FOR: U.S. Army Medical Research and Materiel Command
Fort Detrick, Maryland 21702-5012

REPORT DOCUMENTATION PAGE

Form Approved
OMB No. 0704-0188

1. REPORT DATE *(DD-MM-YYYY)*	**2. REPORT TYPE**	**3. DATES COVERED** *(From - To)*
01-01-2007	Final	01 Jan 04 – 31 Dec 06

4. TITLE AND SUBTITLE
The Role of the Caspase-8 Inhibitor FLIP in Androgen-Withdrawal Induced Death of Prostate Epithelium

5a. CONTRACT NUMBER

5b. GRANT NUMBER
W81XWH-04-1-0149

5c. PROGRAM ELEMENT NUMBER

6. AUTHOR(S)
John Krolewski, MD-PhD; Kent Nastiuk, PhD

E-Mail: jkrolews@uci.edu

5d. PROJECT NUMBER

5e. TASK NUMBER

5f. WORK UNIT NUMBER

7. PERFORMING ORGANIZATION NAME(S) AND ADDRESS(ES)
University of California
Irvine CA 92679-7600

8. PERFORMING ORGANIZATION REPORT NUMBER

9. SPONSORING / MONITORING AGENCY NAME(S) AND ADDRESS(ES)
U.S. Army Medical Research and Materiel Command
Fort Detrick, Maryland 21702-5012

10. SPONSOR/MONITOR'S ACRONYM(S)

11. SPONSOR/MONITOR'S REPORT NUMBER(S)

12. DISTRIBUTION / AVAILABILITY STATEMENT
Approved for Public Release; Distribution Unlimited

13. SUPPLEMENTARY NOTES

14. ABSTRACT:
Secretory prostatic epithelial cells undergo apoptosis in response to androgen deprivation. Similarly,metastatic prostate cancers, which resemble secretory epithelium, also undergo apoptosis following androgen deprivation. Recent evidence suggests that death receptor signaling is required for prostate epithelial cell death following androgen withdrawal. We sought to extend this observation by investigating the role of death receptor signaling components in models of prostate epithelial cell death. Preliminary experiments suggest that FLIP can inhibit apoptosis of prostate epithelial cells. FLIP is an enzymatically inactive version of pro-caspase-8 which negatively regulates cell death, apparently via a dominant- negative mechanism. Based on our preliminary data, we hypothesize that FLIP is a key regulator of prostate apoptosis in response to androgen withdrawal. To address our hypothesis we propose a systematic approach involving, sequentially, correlative (aim 1), functional (aim 2) and mechanistic (aims 3 and 4) experiments. The specific aims are: i) correlate the pattern of FLIP expression with prostate epithelial cell death; ii) assess the functional consequences of forced FLIP expression on prostate epithelial apoptosis; iii) determine which death receptor pathway is involved in prostate epithelial cell death and iv) determine if androgens regulate the level of FLIP expression at the level of gene transcription.

15. SUBJECT TERMS
None provided

16. SECURITY CLASSIFICATION OF:			**17. LIMITATION OF ABSTRACT**	**18. NUMBER OF PAGES**	**19a. NAME OF RESPONSIBLE PERSON**
a. REPORT	**b. ABSTRACT**	**c. THIS PAGE**			USAMRMC
U	U	U	UU	60	**19b. TELEPHONE NUMBER** *(include area code)*

Table of Contents

INTRODUCTION: Our long term goal is to identify the molecular events which trigger androgen withdrawal induced apoptosis (AWIA), in order to discover novel targets for prostate cancer therapy. The studies focus on FLIP, an inactive homologue of caspase-8, which inhibits apoptosis. Based on our preliminary studies, we hypothesize that FLIP plays a key role in AWIA. Specifically, we propose that FLIP protein levels are transcriptionally down-regulated following androgen withdrawal, permitting the activation of one or more death receptor signaling pathways.

PROGRESS REPORT:

Task 1. Correlate the decline in FLIP expression with the onset of prostate epithelial cell death (months 1-6).

- 1.1 Employ affinity precipitation and immunoblotting to measure FLIP protein levels in apoptosing rat prostate glands.
- 1.2 Use immunohistochemistry and *in situ* hybridization to determine the spatial (cell-type specific) pattern of FLIP expression in apoptosing rat prostate glands.
- 1.3 Measure the levels of FLIP mRNA (by quantitative RT-PCR) and protein (by affinity precipitation and immunoblotting) in NRP-152 cells induced to apoptose by TGFß.

Results: We previously reported having found that FLIP protein levels decline by 24 hours post-castration, before the onset of AWIA in the prostates of castrated rats. This data is shown in Fig. 1 of the Cornforth manuscript in the Appendix (**task 1.1**). We expect that FLIP mRNA and protein levels will be mainly modulated in apoptosing secretory epithelium, rather than in apoptosis-resistant basal epithelial and stromal cells, but have not yet undertaken the studies to confirm this (**task 1.2**). Since differentiation sensitizes NRP-152 cells to TGFß killing, our hypothesis suggests that both FLIP mRNA and protein levels should decline in terminally differentiated NRP-152 cells. Indeed, immunoblots of NRP-152 cells undergoing differentiation show a complex regulation, with an initial decline in FLIP protein levels, followed by an increase within 24 hours. TGFß blocks this later increase in FLIP protein levels. FLIP mRNA levels are similarly reduced through 72 hours of TGFß treatment (see appendix, Nastiuk (a) Figs. 1, 7 and Fig. 1 of the appendix) (**task 1.3**).

Task 2. Assess the functional consequences of forced FLIP expression on prostate epithelial apoptosis (months 1-36).

- 2.1 Create NRP-152 cells expressing an inducible FLIP transgene and confirm our preliminary observation that FLIP overexpression inhibits TGFß induced apoptosis of this immortalized prostate epithelial cell line.
- 2.2 Generate an adenovirus expressing FLIP-IRES-GFP, infect rat prostate glands and determine if constitutive FLIP over-expression inhibits castration induced prostate epithelial cell death.
- 2.3 Create inducible FLIP transgenic mice and determine if FLIP over-expression inhibits castration induced prostate epithelial cell death.

Results: Inducible expression constructs in NRP-152 cells have proven unsuitable due to the loss of TGFß responsiveness during selection of the ecdysone inducible clones. We therefore isolated additional constitutively expressing FLIP short NRP clones to extend our analysis (see Nastiuk (a) Fig. 4). Forced expression of FLIP short inhibits TGFß induced cell death in NRP-152 cells and the inhibition is dependent on the level of FLIP expression. Clones expressing FLIP short fail to show the increased caspase activity that accompanies TGFß treatment of control NRP-152 cells (**task 2.1**) (see Nastiuk (a) Figs. 1, 3 and 4). Additionally, we have begun a new round of isolation of tetracycline-inducible NRP-152 clones in order to revisit whether acute modulation of FLIP, as well as modulators of FLIP, such as AKT kinase activity, affect prostate cell survival. Adenoviruses expressing GFP alone and both the long and short forms of FLIP with an IRES-driven GFP cassette have been produced (Figure 2). Unfortunately, the FLIP long expressing adenovirus does not infect either rat or human prostate cells in culture (data not shown). The FLIP short adenovirus does infect NRP-152 (and other) prostate cell lines, but induces apoptosis at high MOI (Figure 3A). Lowering the MOI reduces the proportion of GFP positive cells, as expected (appendix Figure 3B and C), but at these reduced MOI levels, while there is no increased adenoviral-induced cell death, there is also only partial protection of the NRP-152 cells from TGFß1-induced cell death. When 50% of the cells are infected (MOI=4), only ~33% of the infected cells die, versus 75% of uninfected cells (appendix Figure 3D, 3E). Due to the low infectivity and toxicity of the adenoviral constructs, we have not infected rat prostate *in vivo* (**task 2.2**). Because we have not been able to characterize inducible constructs *in vitro*, we have not yet begun creating a mouse line with inducible expression of a FLIP transgene (**task 2.3**).

Task 3. *Examine the mechanism of FLIP action by determining which death receptor pathway is inhibited by FLIP during prostate epithelial apoptosis (months 24-36).*

- 3.1 Determine if Fas and/or TRAIL KO mice are resistant to, or show a reduction in the extent of, castration induced prostate cell death.
- 3.2 Determine if recombinant death receptor ligands (FasL and TRAIL) induce cell death in NRP-152 cells and primary prostate epithelial cells.

Results: Initial experiments using wild-type mice were technically unsatisfactory due to excessive variability derived from the difficulty in dissecting the prostate lobes from the surrounding tissue. We have therefore developed an MRI method with a 7 Tesla small animal MRI since it allows us to more precisely make volume measurements of the organ and to follow the same animal over time, as it is non-invasive. In our submitted manuscript, we demonstrate the general reproducibility of the MRI measurements in assessing the size of intact prostates (Nastiuk (b) Fig. 1) and the involution of the prostate (Nastiuk (b) Fig. 2). We further refined the MRI methodology to suppress the signal due to the surrounding fat, and this allowed us to distinguish the dorsal and lateral from the ventral lobe of the mouse prostate (Nastiuk (b) Fig. 3) and used this to measure the lobe-specific castration-induced regression and subsequent re-growth of the prostate (Nastiuk (b) Figs. 4, 5). We have assessed the rate

of castration-induced regression of the mouse prostate in TRAIL -/- mice and age- and genotype-matched controls. Absence of TRAIL significantly slows the castration induced regression of the mouse prostate (Fig. 4) (**task 3.1**). We have demonstrated that recombinant FasL and TRAIL will induce apoptosis in NRP cells (Nastiuk (a) Figs. 5B and 6C, respectively), but while Fas-Fc, DR4-Fc and DR5-Fc block FasL or TRAIL-induced death in Jurkat cells (Nastiuk (a) Figs. 5B, 6A-B), they fail to block TGFß-induced death in NRP cells (Nastiuk (a) Figs. 5C-D, 6D-F). While we produced rat Fas-Fc, we used human DR4 and DR5 reagents in these studies. We therefore produced rat DR5-Fc protein, as we did for the rat Fas-Fc, to rule out the possibility of inter-species variability resulting in the lack of effect of blocking TRAIL signaling in NRP-152 cells reported in the manuscript. Testing of this reagent's activity blocking TRAIL induced cell death in rat prostate cells is currently underway and will be followed by blocking of TGFß-induced cell death. We have not yet undertaken similar studies in primary prostate epithelial cells (**task 3.2**).

Task 4. Characterize androgen regulation of FLIP expression in the androgen-responsive cell line LNCaP.

- 4.1 Use immunoblotting, RT-PCR and reporter gene assays to determine if androgen–mediated regulation of FLIP occurs at the level of gene transcription.

Results: We have observed androgen mediated modulation of FLIP protein in LNCaP cells and predict that the FLIP gene is regulated by androgen at the level of gene transcription (see Cornforth manuscript in appendix). We have found that the regulation of FLIP is dependent on the PTEN (and hence AKT) state of the cells, and that in LNCaP cells, which lack PTEN, the PI3K inhibitor LY294002 is required to see modulation of FLIP protein by androgens (Cornforth Figs. 2, 3). These effects are also apparent at the mRNA levels of FLIP, where both androgens and LY294002 each repress FLIP in LNCaP cells, but in combination they cooperate to increase FLIP (Cornforth Fig. 4). We find androgen regulation of several reporter constructs driven by portions of the FLIP promoter in LNCaP cells (Cornforth Fig. 5), and in addition find an AKT regulated Forkhead transcription factor (FOXO3a) binding site is important in regulating both FLIP levels and transcription from the FLIP promoter (Cornforth Figs 5, 6). Modulating the FLIP levels via both pathways leads to differential sensitivity to apoptosis induction via TRAIL in the LNCaP cells *in vitro* (Cornforth Figs. 7, 8). Additionally, we have also observed a role for Akt activators such as insulin in modulating FLIP expression in the rat prostate cell line NRP-152 (Nastiuk (a) Fig. 7). (**task 4.1**).

KEY RESEARCH ACCOMPLISHMENTS:

- Define the complex regulation of FLIP protein in differentiating NRP cells
- Isolate and characterize additional FLIP short expressing NRP clones
- Production of adenoviruses expressing rat FLIP short and long with IRES-GFP
- Production of rat TRAIL blocking fusion protein (DR5:Fc)
- Developed MRI methodology to measure prostate volume changes in the same animal over time.
- Demonstrate importance of AKT signaling in regulating FLIP protein levels
- Demonstrate androgen and FOXO3a regulation of transcription from the human FLIP promoter

REPORTABLE OUTCOMES:

1. Presentation at the UCI Cancer Center retreat, 11/04
2. Presentation at the UCI Campuswide Cancer Symposium, 5/05
3. Manuscript submitted to Molecular Cancer Research, 8/05
4. Manuscript submitted to Oncogene, 8/06
5. Manuscript submitted to Biomed Central Urology, 12/06
6. Presentation at the UCI Cancer Center retreat, 11/06
7. Production of two novel adenoviruses, rat FLIP short and long
8. Production of novel TRAIL blocking reagent, rat DR5:Fc
9. Funding applied for: DOD PRCP, NIH RO1 (NCI)

CONCLUSIONS: We continue to make good progress in overcoming the inherent problems working with normal rodent prostate biology. The shifting phenotype during selection of clones of NRP cells for isolation of inducible FLIP clones made it a less desirable alternative than isolation of additional constitutively expressing clones to characterize TGFß-induce apoptosis. The small size and interdigitated nature of the mouse prostate made characterizing AWIA much less reliable than in the rat. We therefore developed the MRI method, which is more precise than dissecting and weighing, since we are able to sample the same animal over time, rather than the mean of groups of mice sacrificed at different times, and are able to monitor both the regression and androgen stimulated regrowth in the same animal. Utilizing this methodology, we were able to discern a small but significant effect of TRAIL on normal AWIA *in vivo*. Regulation of FLIP in the human prostate cancer cell line LNCaP appears to be under control of both androgens and the growth factor signaling pathway involving AKT acting via Foxo3a. We expect that prostate cells with wild-type levels of PTEN will show more consistent regulation of FLIP by androgens.

REFERENCES: None

APPENDIX: See attached table of contents

APPENDIX

Figure 1 FLIP protein levels decline following castration

Figure 2. Production and expression of FLIP expressing Adenovirus.

Figure 3. Adenoviral FLIP short (AdF_{SH}) expression kills NRP-152 cells.

Figure 4. MRI documents involution of TRAIL -/- mouse prostate following castration.

MANUSCRIPTS:

Nastiuk (a) (submitted to Molecular Cancer Research)

Nastiuk (b) (submitted to BMC Urology)

Cornforth (submitted to Oncogene)

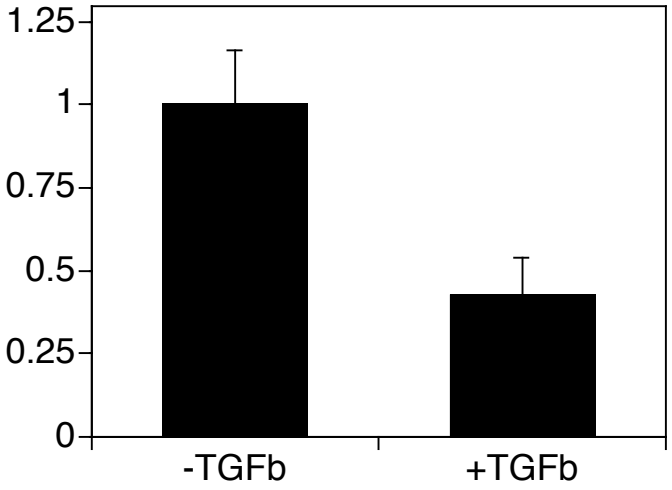

Appendix Figure 1. Reduction in FLIP mRNA after TGFß treatment. NRP-152 cells were treated for 72 hours with 5ng/ml TGFß and RNA isolated, reverse transcribed, and FLIP and Actin mRNA levels assessed using a Lightcycler. Bars represent mean FLIP/Actin mRNA, normalized to untreated control (n=4, +/- s.e.)

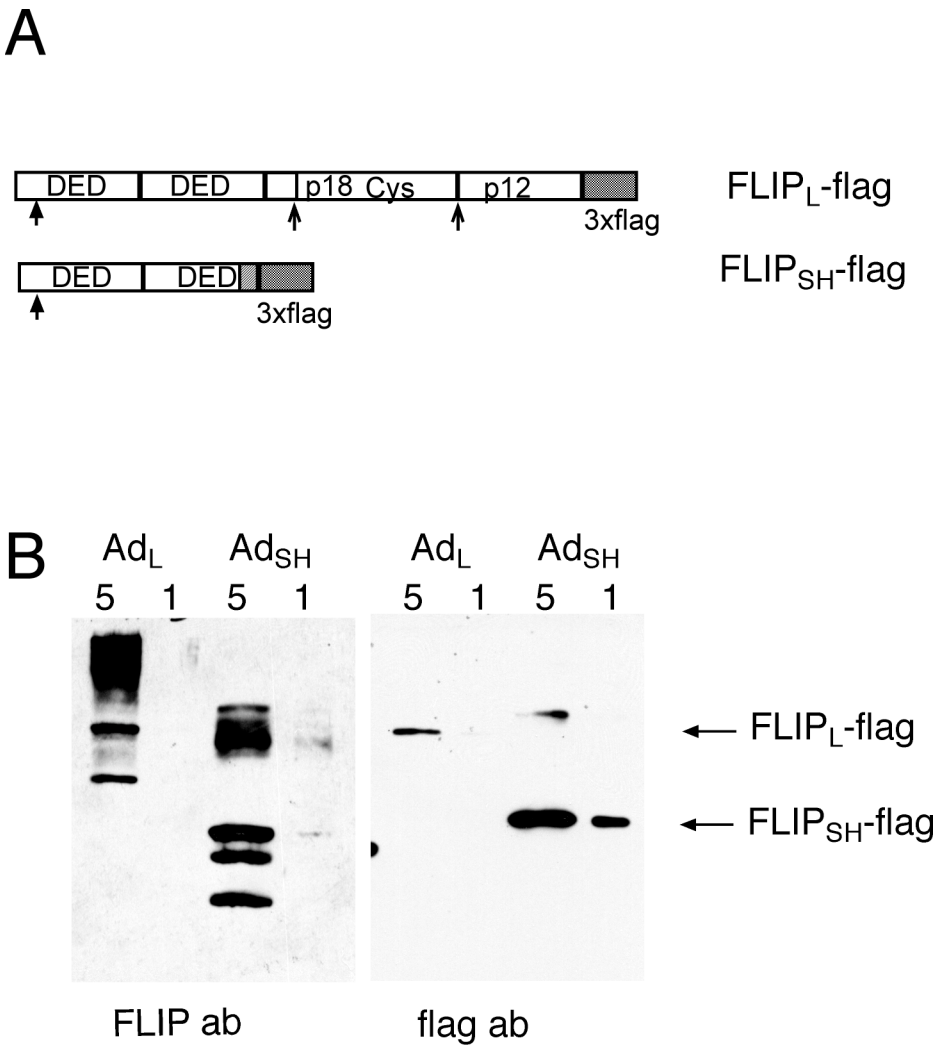

Appendix Figure 2. Production and expression of FLIP expressing Adenovirus. A. Diagram of FLIP long (top) and short (bottom) Virus was prepared by flag-tagging the rat cDNAs and inserting them in an adenovirus under control of the CMV promoter and followed by an IRES-GFP cassette. B. 293 cells were infected with either the FLIP long (AD_L) or short (Ad_{SH}) at the indicated MOI. After 24 hours infection, the cell lysate was examined by SDS-PAGE immunoblotting with either the rat FLIP or flag antibodies (indicated below).

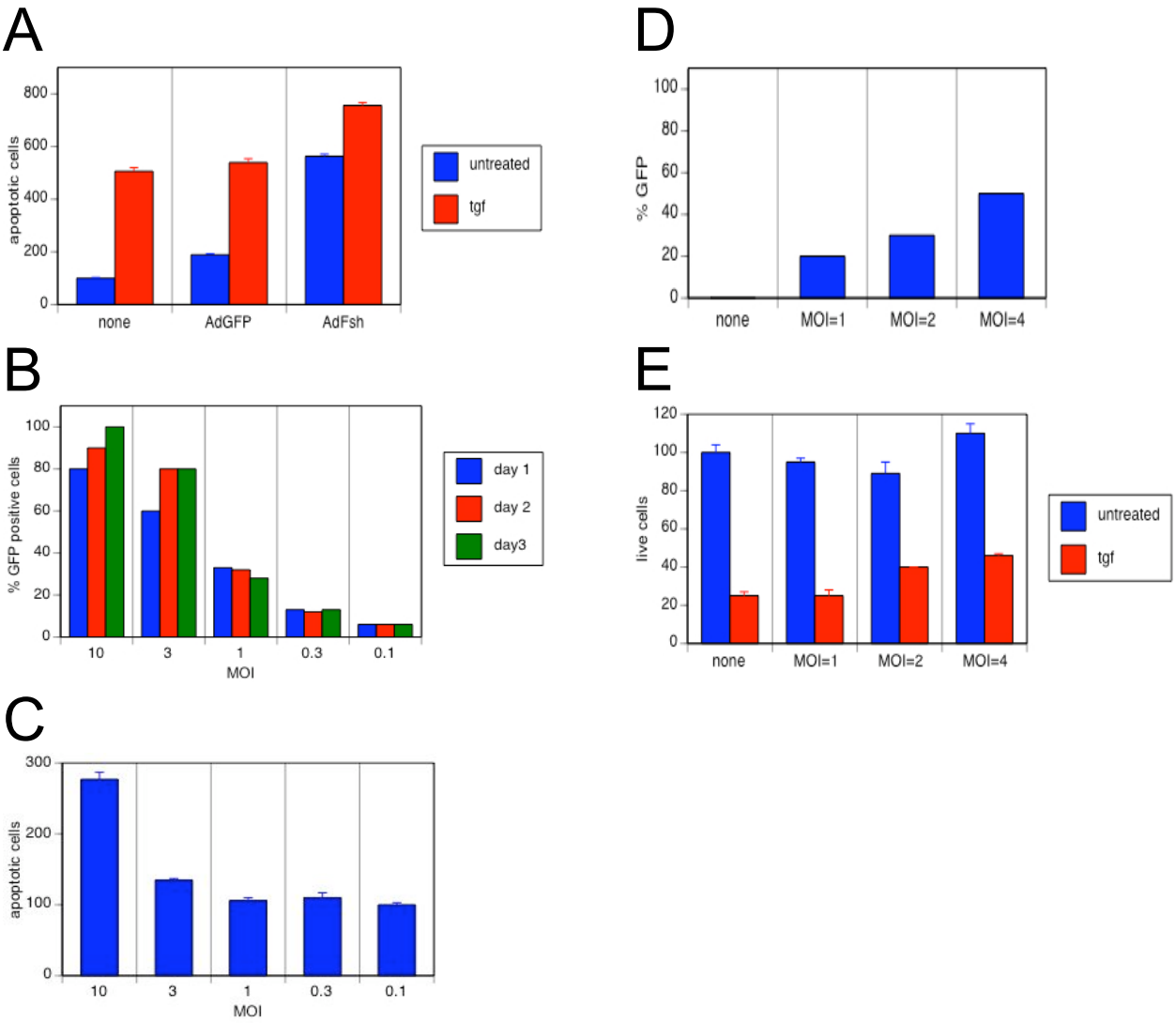

Appendix Figure 3. Adenoviral FLIP short (AdF_{SH}) expression kills NRP-152 cells. A. NRP-152 cells were left uninfected, or infected (MOI=20) with the GFP expressing control virus or FLIP short expressing virus and treated with TGFß1 for 72 hours. Apoptotic cells as a percentage of the untreated, uninfected control. B, C. Varying the MOI of AdF_{SH} infection of NRP-152 cells from 10 to 0.1 resulted in reduction in the percentage of GFP positive cells and viral-induced apoptosis (as a percentage of the cells infected at MOI=0.1). D, E, F. NRP-152 cells infected with AdF_{SH} at MOI=1 to MOI=4 were partially protected from the apoptosis-inducing effects of TGFß1. 72 hours after TGF1 addition, live cells were counted and are shown as a percentage of the uninfected, untreated control cell number.

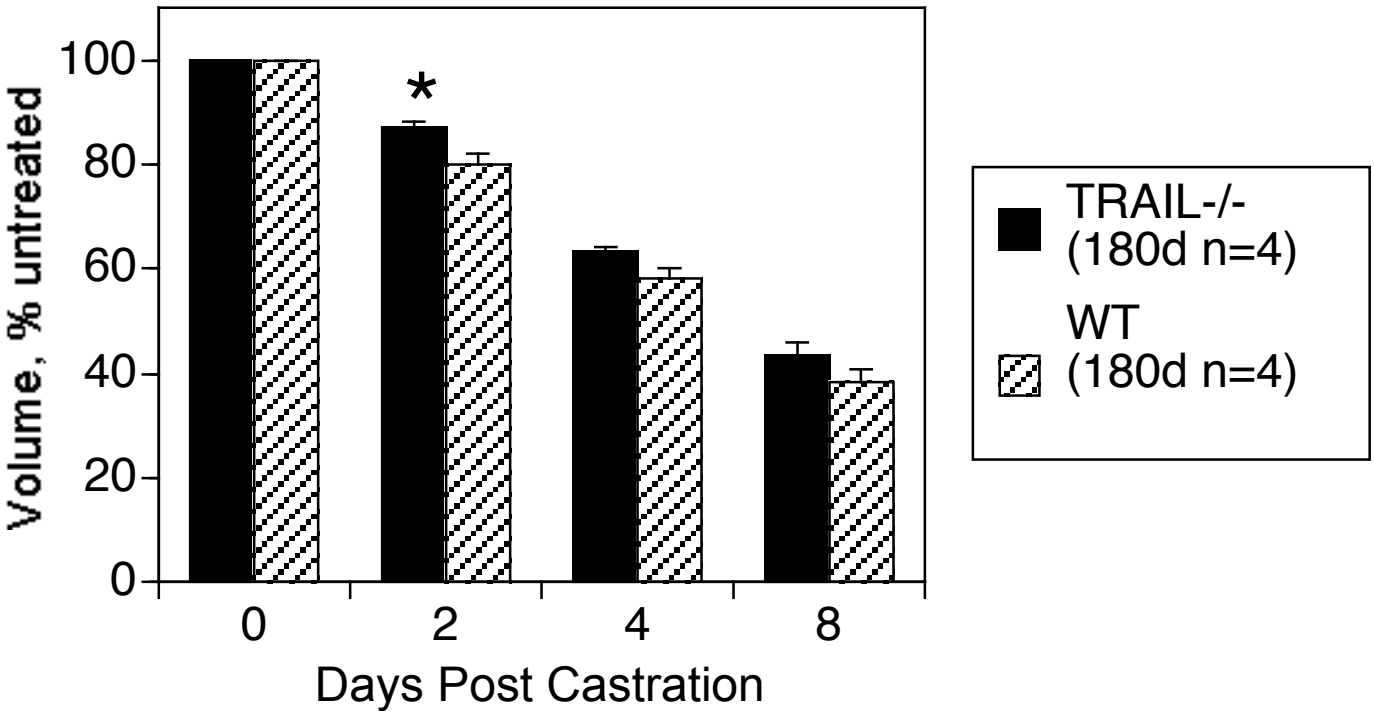

Appendix Figure 4. Regression of prostate following castration. Prostate volume of TRAIL -/- and age-matched WT mice was determined by high resolution MRI at the indicated times . Bars represent mean total prostate volume, normalized to untreated control (n=4, +/- s.e.). Asterix: $p<0.02$

FLICE-like inhibitory protein blocks TGFß1 induced caspase activation and apoptosis in prostate epithelial cells

Kent L. Nastiuk[1], Kiwon Yoo[1], Karen Lo[1], Kevin Su[1], Patricia Yeung[1], Julia Kutaka[1], Andrew Cornforth[1], David Danielpour[3] and John J. Krolewski[*,1,2]

[1]Department of Pathology and Laboratory Medicine
[2]Chao Family Comprehensive Cancer Center
University of California, IRVINE
Irvine, CA 92697, USA

[3]Division of General Medical Sciences - Oncology
Case Western Reserve University
Cleveland, OH 44106, USA

***Correspondence:**
JJ Krolewski, Department of Pathology and Laboratory Medicine, School of Medicine, UC Irvine, Medical Sciences I D450, Irvine, CA 92697-4800; E-mail: jkrolews@uci.edu
Phone: 949-824-4089
Running Title: FLIP blocks apoptosis of prostate epithelial cells
Key Words: FLIP, apoptosis, TGFß, caspase, prostate epithelial cells, NRP-152

Abstract

Androgen withdrawal induces regression of human prostate cancers, but such cancers eventually become androgen independent and metastasize. Thus, deciphering the mechanism of androgen-withdrawal induced apoptosis (AWIA) is critical to designing new therapies for prostate cancer. Previously we demonstrated that in the rat, castration-induced apoptosis is accompanied by a reduction in the expression of the apical caspase inhibitor FLIP (FLICE-like Inhibitory Protein). To test the functional role of FLIP in inhibiting prostate epithelial cell apoptosis, we employed the rat prostate epithelial cell line NRP-152 (NRP). NRP cells differentiate to a secretory phenotype in low-mitogen media and then undergo apoptosis following TGFß1 addition, mimicking AWIA. NRP cells were stably transfected with constitutively expressed FLIP. NRP clones expressing higher levels of FLIP were refractory to TGFß1 induced apoptosis. TGFß1 induced caspase-3 activity is proportional to the level of cell death and inversely proportional to the level of FLIP expression in various clones. Moreover, neither caspase-3 nor PARP is cleaved in clones expressing high level FLIP. To assess whether a death receptor (DR) ligand is involved in TGFß1 induced apoptosis, we used DR-Fc chimeric proteins that block ligand-receptor interactions. Neither Fas-Fc, DR4-Fc nor DR5-Fc blocked TGFß1 induced cell death. However, insulin increases FLIP and inhibits NRP death, suggesting that FLIP blocks other DR-ligands and/or mitochondrial apoptosis.

Introduction

Androgens regulate the growth of both normal and neoplastic prostate, and androgen signaling blockade is the primary treatment for late stage prostate cancer. Thus, there is an urgent need to understand the molecular events regulating androgen withdrawal-induced apoptosis (AWIA). As in humans, androgens promote mitosis and differentiation of rodent prostate ductal epithelium, and further, appear to inhibit apoptosis of differentiated cells (1). After androgen ablation in rodents, the balance between mitosis and apoptosis is disrupted, and within two days markers of apoptosis, such as fragmentation of chromosomal DNA, are evident (2, 3). This wave of cell death results in the involution of the prostate gland (4).

A variety of evidence supports the view that TGFß1 is a paracrine and/or autocrine mediator of AWIA in the intact animal. AWIA is accompanied by an increase in TGFß1

mRNA, and the kinetics of mRNA induction closely parallel those of AWIA (5). Additionally, there is a concomitant rise in the expression of the RI and RII subunits of the TGFß1 receptor (6) as well as phosphorylated Smad2, a key downstream mediator of TGFß1 (4). A dominant negative form of TGFß-RII blocks TGFß1 induced differentiation and cell death (7, 8). Finally, administration of TGFß1 to rats results in apoptosis of the prostate (5, 9). Although the mechanism of TGFß1 action is unclear (it might involve transcriptional effects on pro- and anti-apoptotic proteins (10)), one potential downstream target is the family of death receptor (DR) signaling ligands.

Four extracellular ligands of the TNF family initiate apoptosis through the DRs: TNF, TRAIL, TWEAK, and FasL. The best characterized of these DR ligands is FasL, which signals through the Fas receptor to initiate a cascade of proximal and then distal caspase activation, release of the mitochondrial contents and further caspase activation. This leads to fragmentation of chromosomal DNA, various proteins, and cellular membranes, resulting in cell death (11, 12). We have previously shown that one inhibitor of the DR pathways, FLICE-like inhibitory protein (FLIP), is down-regulated in the rat prostate following castration (2). FLIP is an inactive homologue of caspase-8, an apical caspase activated in DR signaling. Like caspase-8, FLIP can be recruited to DRs following ligand binding, via the adaptor molecule FADD. Elevated levels of FLIP can displace caspase-8 from the activated DR complex, acting as a dominant inhibitor of caspase-8 and thereby preventing the activation of distal caspases and cell death (13). Surgical specimens from normal human prostate, as well as both androgen responsive and unresponsive tumors, express Fas and FasL (14, 15). TRAIL induced apoptosis can be inhibited by FLIP (16, 17). TRAIL induces apoptosis of both normal prostate epithelial cells (18) and prostate cancer cell lines (19, 20) but many cancers are resistant to TRIAL-induced apoptosis due to over-expression of FLIP. This resistance can be reversed by blocking FLIP expression using chemotherapeutics (21) or siRNA (22-25).

To test the functional role of FLIP in inhibiting prostate epithelial cell apoptosis, we employed the immortalized, non-tumorigenic rat prostate epithelial cell line NRP-152 (NRP) (26). When grown in mitogen-rich media these cells resemble prostate basal epithelia and divide rapidly. In mitogen-poor media, growth is suppressed as the cells differentiate into a secretory phenotype (27). The ability of NRP cells to replicate as basal-like epithelial cells and subsequently differentiate into secretory-like epithelial cells *in vivo* and *in vitro* suggests this cell line is an excellent model for normal prostatic epithelium. It is the secretory epithelium of the prostate which apoptoses after androgen withdrawal. Importantly, the physiologic process of AWIA can be mimicked in NRP cells *in vitro*, by the addition of TGFß1 to cultures previously differentiated in mitogen-poor media. NRP cells maintained in mitogen-rich media are resistant to TGFß1 induced apoptosis (28). This is due at least in part to activation of the Akt/mTOR pathway, which suppresses Smad3 activation (29). Our previous observation that castration-induced down-regulation of FLIP in the rat prostate immediately precedes the onset of apoptosis, suggested that FLIP might have a functional role in regulating the apoptosis of prostate epithelium that occurs following androgen withdrawal. The current report tests this possibility, employing TGFß1 induced apoptosis of NRP cells as a model for AWIA in the rat prostate.

Results

NRP-152 cells grown in rich media (GM2), then re-plated in low growth factor media (GM3), rapidly differentiate to a luminal (secretory) epithelial phenotype, both morphologically and biochemically (27). The proliferation of these cells slows markedly from a doubling time of less than a day to more than three days (Figure 1a, cross-hatched bars and data not shown (DNS)) but they do not apoptose (Figure 1a, squares). If, after 3 h in differentiation media, the cells are treated with 5 ng TGFß1/mL, the adherent live cells decline by about half at two

days while the apoptotic cells increase ten-fold relative to the untreated controls (Figure 1A, black bars and circles). Nucleosomal cleavage of DNA isolated after TGFß1 treatment shows that the apoptosis is evident as early as 10 h after TGFß1 addition (Figure 1b). Within 6 h, the activity of caspase-3 in TGFß1 treated cells is elevated relative to untreated NRP-152 cells. Caspase-3 activity continues to rise through 36 h TGFß1 treatment (Figure 1c). Immunoblots of nuclear extracts of NRP cells either untreated or treated with TGFß1 for up to 72 h (Figure 1d), show that one substrate of caspase-3, poly(ADP-ribose)polymerase (PARP), is also cleaved in the TGFß1 treated cells with a maximum at 36 h treatment. The initial high level of PARP cleavage at 12 h is not likely due to TGFß1 effects on cells, but to cells that fail to differentiate and die as a result of the low level of growth factors in the differentiation media. Since we have previously found that FLIP is reduced during rat prostate apoptosis, cytoplasmic protein isolated from a combination of adherent and floating cells at each time-point was examined by immunoblotting for FLIP. FLIP protein is low when the NRP cells are re-plated in differentiation media and subsequently increases 24-60 h after differentiation (Figure 1e). Differentiating NRP cells treated with TGFß1, in contrast, express low FLIP levels for up to 48 h following treatment.

The decline in FLIP levels in response to TGFß1 may leave NRP cells more vulnerable to apoptosis. To test this hypothesis, we transfected a constitutively expressed FLIP gene into NRP cells and selected clonal lines expressing varying levels of FLIP. FLIP is expressed in two isoforms: FLIP long ($FLIP_L$) which has two DED domains at the amino-terminus, followed by a caspase domain containing inactivating mutations, and FLIP short ($FLIP_S$), which contains only the two DED domains. Both $FLIP_L$ and $FLIP_S$ can be detected by our DED-directed anti-FLIP antibody (DNS), but only the long form is found in extracts of NRP cells. High level over-expression of $FLIP_L$ has been previously reported to induce apoptosis via a mechanism that is poorly understood (30-32). Therefore, we transfected NRP cells with either a HA-tagged $FLIP_S$ construct, or the corresponding empty vector, and isolated clonal lines. To assess apoptotic response, cells were differentiated in GM3 and treated with TGFß1. Differentiated parental NRP cultures treated with TGFß1 contain more than three times as many apoptotic cells as untreated differentiated cultures (Figure 2a, bar labeled P). Cultures from clones transfected with vector alone display somewhat less apoptotic response to TGFß1 induced cell death (Figure 2a, V1; Figure 4a, V2 and DNS). This may be due to extended passaging during the selection process, which can produce clones partially resistant to TGFß1 (27). Of 48 G418-resistant clones screened for $FLIP_S$, one showed high and two others very low levels of anti-HA immunoreactivity (Figure 2b and DNS). When the resistant but non-expressing clones were assessed for TGFß1 induced apoptosis, a range from 150-350% (relative to the untreated, differentiated control; see Materials and Methods) was seen (Figure 2a). Two clones expressing low levels of FLIP (14 and 42) had a level of apoptosis equal to 250% of the untreated control, while the one clone (12) expressing a high level of $FLIP_S$ showed no increase in TGFß1 induced apoptosis (Figure 2a). Similarly, when DNA was isolated from these clones 72 h after TGFß1 treatment, internucleosomal cleavage was evident in samples from parental (P), vector-transfected (V), low expressing (14, 42) and non-expressing (32, 37) clones, but there was no cleavage of the DNA isolated from the clone (12) expressing high levels of $FLIP_S$ (Figure 2c).

Cytosolic extracts were prepared from differentiated clones and caspase-3 enzymatic activity was determined (Figure 3b). The induction of caspase activity in TGFß1 treated versus untreated cells ranged from 5- to 15-fold in parental (P), vector only (V1), and low expressing clones (32, 37). The clone (12) expressing high levels of $FLIP_S$ showed no induction of caspase-3 activity (Figure 3b). The level of induction of caspase-3 activity correlated closely with the level of TGFß1 induced apoptosis (compare Figures 3a and 3b).

The extracts used in Figure 3b were immunoblotted using an antibody that detects both full-length caspase-3 (32 kD) and its active fragment (17 kD). The top panel of Figure 3c shows that TGFß1 treated and untreated extracts have approximately equal amounts of caspase-3, but a long exposure of the lower portion of the blot shows that the 17 kD fragment is induced in extracts from all of the TGFß1 treated clones except clone 12 (Figure 3c, lower panel). Similarly, the caspase-3 substrate PARP is cleaved from 117 kD to an 84 kD fragment after TGFß1 treatment in all clones except clone 12 (Figure 3d).

There is a strong correlation between $FLIP_S$ transgene expression, caspase-3 activity and apoptosis for this set of clones, but the variability in TGFß1 response after selection and the lack of response in the low expressing clones suggested that analysis of an additional set of $FLIP_S$ expressing clones might be informative. We therefore isolated an additional set of clones. Two of 48 G418 resistant clones in this second set expressed relatively high levels of $FLIP_S$ (Figure 4b, top panel) with clone 66 expressing several times more $FLIP_S$ than clone 48. Extended exposure of the immunoblot reveals that three additional clones display low level expression (Figure 4b, second panel). Each of these low expressing clones has similar levels of endogenous $FLIP_L$ when normalized to actin (Figure 4b, third and fourth panels). Additional anti-FLIP immunoblots (DNS) demonstrated that clones 48 and 66 expressed $FLIP_S$ at levels approximately equivalent to the level of endogenous $FLIP_L$, while clones 61, 43, 53 produce significantly less of the short isoform relative to the level of the endogenous long isoform. Apoptosis in response to TGFß1 ranged from 280-375% for the vector clones (Figure 4a, V2 and DNS) and non-expressing clones (44, 51 in Figure 4a and DNS). The three low expressing clones had an intermediate level of apoptosis (140-180%) while the clone with a higher level of $FLIP_S$ expression (48) had 130%, and the highest expressor (66) only 80%, of the TGFß1 induced apoptosis relative to untreated controls (Figure 4a). Again, caspase-3 activity was highly induced (~15-fold) after TGFß1 treatment of the vector containing and $FLIP_S$ non-expressing clones (Figure 4c). The low expressing clones displayed attenuated induction (~2-fold), while the two high expressors showed no induction of caspase-3 activity (Figure 4c). Induction of PARP cleavage was only seen in the vector containing and the non-expressing clones (V2, 44, 51 in Figure 4d) while there was no TGFß1 induced cleavage in any of the $FLIP_S$ expressing clones. Thus, Figures 2-4 indicate that forced over-expression of $FLIP_S$ protects NRP cells from TGFß1 induced caspase activation and cell death.

FLIP is thought to block DR induced activation of the apical caspases -8 and -10. Since the Fas DR has been implicated in prostate apoptosis (33-35), we sought to determine if TGFß1 induced apoptosis requires Fas signaling, by employing Fas-Fc to block the FasL-Fas interaction. Initial experiments using human Fas-Fc did not block cell death (DNS). Since rat Fas differs from human Fas, a chimera (rFas-Fc) containing a CD5 leader, the extracellular domain of rat Fas fused to Fc and a carboxyl-terminal HA tag was expressed in 293T cells and purified on a protein A column (Figure 5a). Jurkat cells were then used to validate the molecular reagents (Figure 5b). Specifically, treatment with 200 pg/ml of membrane bound FasL (mFasL) induced cell death after 18 h (diagonal striped bars). Further addition of Fc had no effect, while rFas-Fc completely blocked mFasL mediated killing. If TGFß1 induced apoptosis is mediated via the FasL-Fas pathway, the kinetics of death should be similar for mFasL and TGFß1. Indeed, when NRP cells are treated with mFasL, there is very little cell death apparent until 48 h and it is maximal at 72 h (Figure 5c and DNS). In addition, NRP cells are less sensitive than Jurkat cells to mFasL, with a ten-fold higher dose (2 ng/ml) required for complete NRP killing (DNS). The addition of rFas-Fc blocks mFasL induced killing (Figure 5c, compare black and horizontally striped bars), but does not effect killing at two doses of TGFß1 (1 ng/ml, diagonally striped bars; 5 ng/ml, checkered bars). Similarly, neither 5- nor 25-fold

increases in the amount of rFas-Fc significantly reduced the apoptosis induced by 1 ng/ml TGFß1 in these cells (Figure 5d).

Since rFas-Fc was unable to block TGFß1 induce apoptosis, we examined whether TRAIL, which acts via FLIP-inhibitable caspase 8 or caspase 10, might be induced by TGFß1 and blocked by FLIP. Specifically, since TRAIL kills neoplastic and normal human prostate epithelial cells (18) via activation of the apical caspases (36), we examined its role in TGFß1 mediated apoptosis. TRAIL can bind two death-inducing receptors, DR4 and DR5, as well as three decoy receptors and OPG (37) and Fc fusions of the extracellular domains of these receptors block TRAIL-induced cell death (18). As in Figure 5, we employed Jurkat cells to demonstrate the utility of DR4-Fc and DR5-Fc. Although treatment with DR4-Fc alone was partially toxic to Jurkat cells, DR4-Fc was able to block TRAIL induced death, particularly at lower concentrations of TRAIL (Figure 6a). DR5-Fc was also able to block TRAIL induced cell death (Figure 6b). TRAIL killed NRP cells but, as was the case for mFasL, only at significantly higher concentrations relative to the dose that was effective in killing Jurkat cells (Figure 6c). Since DR4-Fc and DR5-Fc were most effective blocking lower TRAIL doses, we treated NRP cells with varying doses of TGFß1, from 0.1 ng/ml, which is sub-lethal, up to 5 ng/ml and found the minimum concentration necessary to induce apoptosis is 0.5 ng/ml (Figure 6d-e, solid bars). As was the case for the Jurkat cells, DR4-Fc treatment of NRP cells was partially toxic in the absence of TGFß1 (Figure 6d, bars at far left). However, neither DR4-Fc nor DR5-Fc inhibited TGFß1 induced apoptosis of NRP cells (Figure 6d-e, solid vs. striped bars). Since the two TRAIL receptors might have complementary roles in signaling (38), we also employed DR4-Fc and DR5-Fc in combination, but again observed no effect on TGFß1-induced cell death (Figure 6f).

Finally, we sought to determine if growth factors that modulate the growth and differentiation of NRP cells also regulate FLIP expression. Insulin and epidermal growth factor (EGF) both stimulate NRP proliferation in the presence of 10% fetal bovine serum (26), but only insulin (as well as the related growth factor IGF-1) inhibits the differentiation of NRP cells from the basal to the luminal phenotype (27). Insulin addition to the cell medium during differentiation effectively blocks TGFß1 induced apoptosis as reported previously (28, 29), while EGF addition does not (Figure 7a, striped bars). Both insulin and EGF induce an increase in the level of $FLIP_L$ but the kinetics are distinct. Specifically, when NRP cells are grown in GM3 differentiation media plus insulin, $FLIP_L$ protein levels increase significantly after 6 h (Figure 7b, lanes 3-4) and remain elevated at 24 h and 48 h (Figure 7c, lanes 2 and 6). In contrast, when EGF is added to differentiating NRP cultures, $FLIP_L$ levels rise only slightly after 6 h (Figure 7b, lanes 1-2) before increasing significantly at 24 h and 48 h (Figure 7d, lanes 2 and 6). Figure 1 demonstrated that treatment of differentiated NRP cells with TGFß1 down-regulates $FLIP_L$ protein levels and coordinately induces apoptosis. Similarly, Figure 7c-d (lanes 3-4 and 7-8) shows that TGFß1 reduces $FLIP_L$ expression and induces PARP cleavage, a marker of apoptotic caspase activation. Insulin prevents the TGFß1 induced reduction of $FLIP_L$ at both 24 h (Figure 7c, lanes 1 and 3) and 48 h (Figure 7c, lanes 5 and 7) and effectively prevents PARP cleavage. EGF is not effective at reducing $FLIP_L$ expression and is only partly effective at inhibiting PARP cleavage (Figure 7c, lanes 1,3, 5 and 7). Thus, treatment of NRP cells with these EGF and Insulin during differentiation modulates $FLIP_L$ levels and further demonstrates that TGFß1 induced apoptosis is inversely correlated with the level of $FLIP_L$ expression.

Discussion

Androgen withdrawal induced cell death appears to be mediated, at least in part, by TGFß that is secreted in response to androgen ablation. Significantly, the NRP-152 cell line apoptoses when treated with TGFß1, as demonstrated by caspase activation, DNA fragmentation and a decline in cell number (Figure 1). Since we

previously demonstrated that both FLIP mRNA (2) and protein levels (KLN and JJK, unpublished observations) decline following castration in rats, we sought to determine whether enforced, continuous expression of FLIP would be sufficient to block TGFß1 induced apoptosis of NRP cells. We chose to express $FLIP_S$ since $FLIP_L$ over-expression has been reported to spontaneously induces cell death in some cell lines. While we do not necessarily believe that $FLIP_S$ is the relevant FLIP isoform in NRP cells (indeed we have not detected $FLIP_S$ in NRP cells; see Figure 1) we were concerned that our expression vector might be more potent than the endogenous promoter, running the risk of over-expression. When NRP cells were stably transfected with an HA-tagged, constitutively expressed $FLIP_S$ gene, evidence of TGFß1 induced apoptosis was absent (Figures 2-4). Further, NRP clones expressing very low levels of $FLIP_S$ showed no evidence of apoptosis, while clonal cell lines expressing moderate levels of $FLIP_S$ showed an intermediate phenotype, suggesting the dose of $FLIP_S$ expression is crucial in determining its effectiveness in blocking cell death in normal prostate cells. This stoichiometry dependent effect of $FLIP_S$ is consistent with the idea that this protein acts in a dominant inhibitory manner to block the function of caspase-8.

If $FLIP_S$ antagonizes TGFß1 induced apoptosis by inhibiting caspase-8, both proximal and distal caspase mediated cleavage events should be attenuated. As expected, TGFß1 treatment of untransfected NRP cells induced significant cleavage of both caspase-3 and PARP, a caspase-3 substrate and apoptosis marker, as well as the caspase-3 peptide substrate (Figure 1). However, when we examined caspase activation in TGFß1 treated $FLIP_S$ expressing clones, we found little or no increase in caspase-3 activity (Figures 3-4). Furthermore, neither caspase-3 itself nor PARP are cleaved in the clones expressing intermediate or high levels of exogenous $FLIP_S$ (Figures 3-4 and DNS). Taken together, these data indicate that $FLIP_S$ expressing clones which are refractory to TGFß1 induced cell death are not undergoing key biochemical changes that normally accompany apoptosis in NRP cells.

Proximally, we sought to measure caspase-8 activation, since caspase-8 is the likely target of the anti-apoptotic action of $FLIP_S$. In other TGFß1 sensitive human cells, immunoblotting of treated cells with an antibody directed against human caspase-8 detected a slight increase in the caspase-8 cleavage while enzymatic assays revealed a small increase in caspase-8 activity (39). Unfortunately, neither this human antibody nor other antibodies tested detect rat caspase-8 active fragments (DNS) and we have not been able to identify a suitably sensitive antibody directed against rat caspase-8. Thus, we also assayed for cleavage of caspase peptide substrates. While we could readily detect an increase in caspase-8 activity at late (36-48 h) time-points, we could not detect activation of either caspase-8 (or –9) at 6, 12 or 18 h following TGFß1 addition (DNS). Moreover, the caspase-8 and -9 activities observed at late time-points were eliminated when we included an inhibitor of caspase-3, which is highly induced in these lysates (Figure 1c) and is known to cross-cleave both the IETD (caspase-8) and LEHD (caspase-9) substrates (DNS). The relatively low levels of TGFß1 induced caspase-8 activity, which may be a result of the comparatively slow onset of cell death in these prostate epithelial cells versus T-cells, prevented us from determining if $FLIP_S$ over-expression can indeed inhibit caspase-8 activity.

Since NRP apoptosis is blocked by $FLIP_S$, and $FLIP_S$ is thought to inhibit apical caspases bound to death receptors, TGFß1 may act by inducing (or stabilizing) the expression of a death receptor ligand. This can be tested by exploiting the observation that fusions between the extracellular domain of a receptor and the immunoglobulin Fc domain block DR ligand induced apoptosis. To determine if FasL is involved in TGFß1 induced NRP apoptosis, we measured cell death in the presence of rFas-Fc, which blocks the interaction between FasL and Fas. While FasL induced apoptosis in NRP cells, rFas-Fc protein failed to block TGFß1 induced NRP cell death (Figure 5). TRAIL is

thought to be a potent inducer of prostate cell death (20) and TRAIL receptors are expressed in normal prostate epithelial cells (18, 40) as well as a variety of prostate cancer cell lines (41, 42). Blocking DR5 rescues TRAIL-induced apoptosis in normal human prostate epithelial cells (18). Although TRAIL induced NRP apoptosis, blocking experiments with two TRAIL receptor-Fc fusion proteins individually or in combination failed to inhibit TGFß1 induced cell death (Figure 6). While our data argue against a role for TRAIL in TGFß1 mediated NRP apoptosis, it remains possible that the human TRAIL receptor-Fc fusions we employed failed to block rat TRAIL signaling because of sequence differences between the human and rat TRAIL receptors. Consistent with this possibility, others have reported that human DR4-Fc inhibits TGFß1 induced apoptosis of human hepatoma cell lines (43). However, there is also precedence for the possibility that FLIP blocks TGFß1 induced apoptosis in a receptor-independent manner. Specifically, TGFß1 treatment of SNU-620 gastric carcinoma cells activates caspase-8 and induces caspase-8 dependent apoptosis, but this effect is not blocked by Fas-Fc nor is it enhanced by FasL (44). Because TGFß1 induced cell death in SNU-620 cells requires functional FADD, FLIP would be expected to act in a dominant inhibitory manner in this cell line. Thus, a similar mechanism could be operative in NRP cells.

Although the remaining DR ligands (TNF and TWEAK) are also potential candidates to mediate TGFß1 regulated cell death, we believe this is unlikely. TWEAK is a relatively inefficient inducer of apoptosis (45) and there are no reports of its activity in prostate epithelial cells. TNF can induce cell death as well as cell survival, dependent in part on the nature of the receptor complexes formed in response to ligand binding (46). While the mechanism controlling the decision to apoptose or survive is unclear, NFκB activation is an important determinant. In most prostate epithelial cells, including normal epithelial cells and the PC-3 and DU145 cell lines, NFκB is activated and TNF does not induce significant apoptosis (47, 48). The LNCaP cell line undergoes apoptosis in response to TNF, but is defective in the regulation of NFκB and therefore may be a poor model for normal prostate epithelium (47). Thus, it seems unlikely that TNF mediates cell death in normal prostate epithelial cells.

Finally, to better understand how the process of NRP differentiation sensitizes cells to TGFß1 induced apoptosis, we investigated the modulation of FLIP expression by mitogens. Insulin and IGF-1 protect against TGFß1 induced apoptosis, while EGF does not (Figure 7 and (29). IGF-1 and insulin, which signal via similar pathways, act in two ways: inhibiting the activation of Smad3, and maintaining the intracellular level of FLIP, even in the presence of TGFß1 (Figure 7). Both insulin and IGF-1 induce Akt phosphorylation, inhibiting the activity of Smad3 (49) and Bad (50), and up-regulating FLIP (Figure 7). Phospho-Akt, but not EGF stimulated phospho-ERK, is associated with an increased proliferative index in prostate tumors (51). This suggests that the resistance of insulin stimulated NRP cells to apoptosis, perhaps acting via sustained expression of FLIP, is reflective of changes in human tumors.

Materials and Methods

Reagents and Antibodies

Caspase substrates (Biomol, Plymouth Meeting, PA), mFasL (UBI, Charlottesville, VA), 'super killer' mouse TRAIL, DR4-Fc and DR5-Fc (Alexis Biochemicals, San Diego, CA), TGFß1 (R&D systems, Minneapolis, MN), anti-actin (AC-10, Sigma, St. Louis, MO), anti-PARP (C2.10, Enzyme Systems, Livermore, CA) were purchased from the indicated suppliers. Antibody against the rat $FLIP_L$ amino-terminal peptide QVEESLDEDEKEC was prepared by immunizing rabbits and then purified by peptide affinity chromatography.

Cell culture, transfection and apoptosis assay

Passage 27 NRP-152 cells were maintained as described (26). Briefly, the cells were cultured in GM2 (Dulbecco's modified Eagle's medium/F12 medium containing 5% fetal bovine serum, 20 ng/ml epidermal growth factor (BD Biosciences, San Jose, CA), 0.1 mM dexamethasone (Sigma), 10 ng/ml cholera toxin (Sigma), and 350 nM insulin (Biosource, Camarillo, CA)) and passaged before

reaching confluence. NRP cells were discarded after 15 passages, except the FLIP expressing clones, which range from 20 to 25 passages after selection. Apoptosis assays were performed in differentiation media (GM3; Dulbecco's modified Eagle's medium/F12 containing 1% calf serum, 15 mM HEPES, and 0.1 mM dexamethasone) using 5 ng/ml TGFß1 or vehicle (4 mM HCl, 1 mg/ml bovine serum albumin).

The rat $FLIP_S$ cDNA was cloned by RT-PCR into pBluescript, transferred to a vector containing a carboxyl-terminal HA tag and then into the KpnI and ApaI sites of pcDNA3.1 (Invitrogen, Carlsbad, CA) to create p-rat$FLIP_S$HA. This plasmid was transfected with Lipofectamine Plus (Life Technologies, Inc., Gaithersburg, MD) and transfectants selected using G418 (GibcoBRL, Grand Island, NY) at 200 ng/ml in GM2.

After TGFß1 treatment, NRP cells that adhere to tissue culture plates after two PBS washes exclude trypan blue, possess nuclei that appear non-apoptotic by DAPI staining, and show no caspase activation by immunoblotting analysis. In contrast, the detached cells are uniformly apoptotic when recovered from the GM3 media and PBS washes. These detachable (floating) cells are apoptotic by DNA laddering, caspase activation by immunoblot analysis, and DAPI nuclear staining (52). Quantification of NRP detachable cells and adherent cells released by trypsin treatment after the PBS washes using a Coulter counter was therefore used as a measure of TGFß1 induced apoptosis of NRP cells. The percent apoptotic cells (% apoptosis) represents the ratio of detachable cells in the TGFß1 treated dishes relative to the untreated control dishes. TGFß1 treatment of differentiated NRP cells induces a three- to four-fold increase in the number of floating cells and, hence, 300-400% apoptosis (for example bars labeled P in Figures 2a and 3a)

DNA isolation and labeling

Attached and floating NRP cells were pooled and DNA was extracted by lysing cells in 7M guanidine hydrochloride followed by further purification using the Wizard system (Promega) as described previously (2). DNA fragments were end-labeled with ^{32}P-ddATP and terminal deoxynucleotide transferase (TdT) as described (53). The labeled DNA was fractionated on a 2% agarose gel and the gel was dried and autoradiographed.

Caspase activity assays

NRP cells were treated with TGFß1 or vehicle for 36 h. Adherent and floating cells were pooled, harvested, washed with PBS and counted. The cells were lysed in 20 mM EDTA, 5 mM Tris, pH 8.0, and 0.5% Triton X-100 to isolate caspase-containing cytoplasm. Extract from 400,000 cells was diluted into 0.1% CHAPS, 50 mM DTT, 50 mM HEPES, pH 7.4, 100 mM NaCl, 1 mM EDTA and 10% glycerol, 50 µM DEVD-pNA (caspase-3 substrate), 100 nM IETD-CHO (caspase-8 inhibitor), 5 nM YVAD-CHO (caspase-1 inhibitor) and incubated at 37˚C. Production of pNA was monitored at 405 nm for 3 h and activity was determined from the slope of the curve in the linear range for each sample. Each sample was assayed in triplicate.

Purification of rat Fas-Fc

Full-length rat Fas was cloned by RT-PCR into pBluescript and the ECD excised and cloned into pB-CD5Lneg1 (54) containing the CD5 leader sequence and the human Fc domain. This construct and the CD5L-Fc only fragment were excised and separately inserted into pMT2T-HA to create pMT2T-ratFasECD-Fc-HA and the corresponding Fc-HA construct. HEK293T cells were transfected with either the rFas-Fc or the Fc only construct and the protein was purified from the media via Protein A (BioRad, Hercules, CA) chromatography.

Cell growth assay

In some cases cell growth was assessed by WST-1 (Boehringer, Mannheim, Germany) conversion to formazan. NRP or Jurkat cells were plated in 96-well plates at 2,000 cells/well in GM3 or 10,000 cells/well in RPMI/10% FBS, respectively. Receptor-Fc protein was added at the indicated concentration at the time of plating. After 3 h, FasL, TRAIL, TGFß1 or vehicle were added, as indicated. After an additional 18 h (Jurkat) or 72 h (NRP), WST-1 was added, plates were incubated at 37˚C and absorbance at 450 nm (less background absorbance at 600 nM) was measured in a microplate reader. Conversion rates were derived from the slope of the curve in the linear range for each sample.

Acknowledgements

This research was supported by grant PC030937 from the US Army Prostate Cancer Research Program.

References

1. Isaacs JT. Antagonistic effect of androgen on prostatic cell death. Prostate 1984;5:545-57.
2. Nastiuk KL, Kim JW, Mann M, Krolewski JJ. Androgen regulation of FLICE-like inhibitory protein gene expression in the rat prostate. J Cell Physiol 2003;196:386-93.
3. Colombel MC, Buttyan R. Hormonal control of apoptosis: the rat prostate gland as a model system. Methods Cell Biol 1995;46:369-85.
4. Brodin G, ten Dijke P, Funa K, Heldin CH, Landstrom M. Increased smad expression and activation are associated with apoptosis in normal and malignant prostate after castration. Cancer Res 1999;59:2731-8.
5. Kyprianou N, Isaacs JT. Expression of transforming growth factor-beta in the rat ventral prostate during castration-induced programmed cell death. Mol Endocrinol 1989;3:1515-22.
6. Kim IY, Ahn HJ, Zelner DJ, Park L, Sensibar JA, Lee C. Expression and localization of transforming growth factor-beta receptors type I and type II in the rat ventral prostate during regression. Mol Endocrinol 1996;10:107-15.
7. Kundu SD, Kim IY, Yang T, Doglio L, Lang S, Zhang X, et al. Absence of proximal duct apoptosis in the ventral prostate of transgenic mice carrying the C3(1)-TGF-beta type II dominant negative receptor. Prostate 2000;43:118-24.
8. Tang B, de Castro K, Barnes HE, Parks WT, Stewart L, Bottinger EP, et al. Loss of responsiveness to transforming growth factor beta induces malignant transformation of nontumorigenic rat prostate epithelial cells. Cancer Res 1999;59:4834-42.
9. Martikainen P, Kyprianou N, Isaacs JT. Effect of transforming growth factor-beta 1 on proliferation and death of rat prostatic cells. Endocrinology 1990;127:2963-8.
10. Coyle B, Freathy C, Gant TW, Roberts RA, Cain K. Characterization of the transforming growth factor-beta 1-induced apoptotic transcriptome in FaO hepatoma cells. J Biol Chem 2003;278:5920-8.
11. Nagata S. Apoptosis by death factor. Cell 1997;88:355-65.
12. Nagata S, Golstein P. The FAS death factor. Science 1995;267:1449-56.
13. Peter ME, Krammer PH. The CD95(APO-1/Fas) DISC and beyond. Cell Death Differ 2003;10:26-35.
14. Xerri L, Devilard E, Hassoun J, Mawas C, Birg F. Fas ligand is not only expressed in immune privileged human organs but is also coexpressed with Fas in various epithelial tissues. Mol Path 1997;50:87-91.
15. Sasaki Y, Ahmed H, Takeuchi T, Moriyama N, Kawabe K. Immunohistochemical study of Fas, Fas ligand and interleukin-1ß converting enzyme expression in human prostatic cancer. Br J Urol 1998;81:852-5.
16. Bin L, Li X, Xu LG, Shu HB. The short splice form of Casper/c-FLIP is a major cellular inhibitor of TRAIL-induced apoptosis. FEBS Lett 2002;510:37-40.
17. MacFarlane M. TRAIL-induced signalling and apoptosis. Toxicol Lett 2003;139:89-97.
18. Nesterov A, Ivashchenko Y, Kraft AS. Tumor necrosis factor-related apoptosis-inducing ligand (TRAIL) triggers apoptosis in normal prostate epithelial cells. Oncogene 2002;21:1135-40.
19. Yu R, Mandlekar S, Ruben S, Ni J, Kong AN. Tumor necrosis factor-related apoptosis-inducing ligand-mediated apoptosis in androgen-independent prostate cancer cells. Cancer Res 2000;60:2384-9.
20. Voelkel-Johnson C, King DL, Norris JS. Resistance of prostate cancer cells to soluble TNF-related apoptosis- inducing ligand (TRAIL/Apo2L) can be overcome by doxorubicin or adenoviral delivery of full-length TRAIL. Cancer Gene Therap 2002;9:164-72.
21. Kelly MM, Hoel BD, Voelkel-Johnson C. Doxorubicin pretreatment sensitizes prostate cancer cell lines to TRAIL induced apoptosis which correlates with the loss of c-FLIP expression. Cancer Biol Ther 2002;1:520-7.
22. Siegmund D, Hadwiger P, Pfizenmaier K, Vornlocher HP, Wajant H. Selective inhibition of FLICE-like inhibitory protein expression with small interfering RNA oligonucleotides is sufficient to sensitize tumor cells for TRAIL-induced apoptosis. Mol Med 2002;8:725-32.
23. Zhang X, Jin TG, Yang H, DeWolf WC, Khosravi-Far R, Olumi AF. Persistent c-FLIP(L) expression is necessary and sufficient to maintain resistance to tumor necrosis factor-related apoptosis-inducing ligand-mediated apoptosis in prostate cancer. Cancer Res 2004;64:7086-91.
24. Rippo MR, Moretti S, Vescovi S, Tomasetti M, Orecchia S, Amici G, et al. FLIP overexpression inhibits death receptor-induced apoptosis in malignant mesothelial cells. Oncogene 2004;23:7753-60.
25. Abedini MR, Qiu Q, Yan X, Tsang BK. Possible role of FLICE-like inhibitory protein (FLIP) in chemoresistant ovarian cancer cells in vitro. Oncogene 2004;23:6997-7004.
26. Danielpour D, Kadomatsu K, Anzano MA, Smith JM, Sporn MB. Development and characterization of nontumorigenic and tumorigenic epithelial cell lines from rat dorsal-lateral prostate. Cancer Res 1994;54:3413-21.
27. Danielpour D. Transdifferentiation of NRP-152 rat prostatic basal epithelial cells toward a luminal phenotype: regulation by glucocorticoid, insulin-like growth factor-I and transforming growth factor-beta. J Cell Sci 1999;112:169-79.
28. Hsing AY, Kadomatsu K, Bonham MJ, Danielpour D. Regulation of apoptosis induced by transforming growth factor-beta1 in nontumorigenic rat prostatic epithelial cell lines. Cancer Res 1996;56:5146-9.

29. Song K, Cornelius SC, Reiss M, Danielpour D. Insulin-like growth factor-I inhibits transcriptional responses of transforming growth factor-beta by phosphatidylinositol 3-kinase/Akt-dependent suppression of the activation of Smad3 but not Smad2. J Biol Chem 2003;278:38342-51.
30. Goltsev YV, Kovalenko AV, Arnold E, Varfolomeev EE, Brodianskii VM, Wallach D. CASH, a novel caspase homologue with death effector domains. J Biol Chem 1997;272:19641-4.
31. Inohara N, Koseki T, Hu Y, Chen S, Nunez G. CLARP, a death effector domain-containing protein interacts with caspase-8 and regulates apoptosis. Proc Natl Acad Sci USA 1997;94:10717-22.
32. Shu HB, Halpin DR, Goeddel DV. Casper is a FADD- and caspase-related inducer of apoptosis. Immunity 1997;6:751-63.
33. Hedlund TE, Duke RC, Schleicher MS, Miller GJ. Fas-mediated apoptosis in seven human prostate cancer cell lines: correlation with tumor stage. Prostate 1998;36:92-101.
34. Hedlund TE, Meech SJ, Srikanth S, Kraft AS, Miller GJ, Schaack JB, et al. Adenovirus-mediated expression of Fas ligand induces apoptosis of human prostate cancer cells. Cell Death Diff 1999;6:175-82.
35. Rokhlin OW, Bishop GA, Hostager BS, Waldschmidt TJ, Sidorenko SP, Pavloff N, et al. Fas-mediated apoptosis in human prostatic carcinoma cell lines. Cancer Res 1997;57:1758-68.
36. Rokhlin OW, Guseva NV, Tagiyev AF, Glover RA, Cohen MB. Caspase-8 activation is necessary but not sufficient for tumor necrosis factor-related apoptosis-inducing ligand (TRAIL)-mediated apoptosis in the prostatic carcinoma cell line LNCaP. Prostate 2002;52:1-11.
37. Truneh A, Sharma S, Silverman C, Khandekar S, Reddy MP, Deen KC, et al. Temperature-sensitive differential affinity of TRAIL for its receptors. DR5 is the highest affinity receptor. J Biol Chem 2000;275:23319-25.
38. Leverkus M, Sprick MR, Wachter T, Denk A, Brocker EB, Walczak H, et al. TRAIL-induced apoptosis and gene induction in HaCaT keratinocytes: differential contribution of TRAIL receptors 1 and 2. J Invest Dermatol 2003;121:149-55.
39. Wallace CS, Withers GS, Weiler IJ, George JM, Clayton DF, Greenough WT. Correspondence between sites of NGFI-A induction and sites of morphological plasticity following exposure to environmental complexity. Brain Res Mol Brain Res 1995;32:211-20.
40. Vindrieux D, Devonec M, Benahmed M, Grataroli R. Identification of tumor necrosis factor-alpha-related apoptosis-inducing ligand (TRAIL) and its receptors in adult rat ventral prostate. Mol Cell Endocrinol 2002;198:115-21.
41. Munshi A, Pappas G, Honda T, McDonnell TJ, Younes A, Li Y, et al. TRAIL (APO-2L) induces apoptosis in human prostate cancer cells that is inhibitable by Bcl-2. Oncogene 2001;20:3757-65.
42. Sridhar S, Ali AA, Liang Y, El Etreby MF, Lewis RW, Kumar MV. Differential expression of members of the tumor necrosis factor alpha-related apoptosis-inducing ligand pathway in prostate cancer cells. Cancer Res 2001;61:7179-83.
43. Herzer K, Ganten TM, Schulze-Bergkamen H, Grosse-Wilde A, Koschny R, Krammer PH, et al. Transforming growth factor beta can mediate apoptosis via the expression of TRAIL in human hepatoma cells. Hepatology 2005;42:183-92.
44. Kim SG, Jong HS, Kim TY, Lee JW, Kim NK, Hong SH, et al. Transforming growth factor-beta 1 induces apoptosis through Fas ligand-independent activation of the Fas death pathway in human gastric SNU-620 carcinoma cells. Mol Biol Cell 2004;15:420-34.
45. Wiley SR, Winkles JA. TWEAK, a member of the TNF superfamily, is a multifunctional cytokine that binds the TweakR/Fn14 receptor. Cytokine Growth Factor Rev 2003;14:241-9.
46. Micheau O, Tschopp J. Induction of TNF receptor I-mediated apoptosis via two sequential signaling complexes. Cell 2003;114:181-90.
47. Chopra DP, Menard RE, Januszewski J, Mattingly RR. TNF-alpha-mediated apoptosis in normal human prostate epithelial cells and tumor cell lines. Cancer Lett 2004;203:145-54.
48. Mukhopadhyay A, Bueso-Ramos C, Chatterjee D, Pantazis P, Aggarwal BB. Curcumin downregulates cell survival mechanisms in human prostate cancer cell lines. Oncogene 2001;20:7597-609.
49. Remy I, Montmarquette A, Michnick SW. PKB/Akt modulates TGF-beta signalling through a direct interaction with Smad3. Nat Cell Biol 2004;6:358-65.
50. Wanke I, Schwarz M, Buchmann A. Insulin and dexamethasone inhibit TGF-beta-induced apoptosis of hepatoma cells upstream of the caspase activation cascade. Toxicol 2004;204:141-54.
51. Ghosh PM, Malik SN, Bedolla RG, Wang Y, Mikhailova M, Prihoda TJ, et al. Signal transduction pathways in androgen-dependent and -independent prostate cancer cell proliferation. Endocr Related Cancer 2005;12:119-34.
52. Chipuk JE, Bhat M, Hsing AY, Ma J, Danielpour D. Bcl-xL blocks transforming growth factor-beta 1-induced apoptosis by inhibiting cytochrome c release and not by directly antagonizing Apaf-1-dependent caspase activation in prostate epithelial cells. J Biol Chem 2001;276:26614-21.
53. Tilly JL, Hsueh AJW. Microscale autoradiographic method for the qualitative and quantitative analysis of apoptotic DNA fragmentation. J Cell Physiol 1993;154:519-26.
54. Zettlmeissl G, Gregersen JP, Duport JM, Mehdi S, Reiner G, Seed B. Expression and characterization of human CD4:immunoglobulin fusion proteins. DNA Cell Biol 1990;9:347-53.

Figure Legends

Figure 1 $FLIP_L$ levels are reduced during TGFß1 induced apoptosis of NRP cells. **(a)** Growth of differentiated NRP cells left untreated (solid bars and square symbol line) or treated with 5 ng/ml TGFß1 (striped bars and circle symbol line). Bars indicate adherent cells (left axis) and lines indicate detached (floating) cells (right axis), each normalized as a percentage of the respective untreated control at 0 h. Error bars correspond to the standard error of the mean. **(b)** Fragmentation of chromosomal DNA in TGFß1 treated NRP cells. Autoradiogram of an agarose gel containing TdT end-labeled nuclear DNA derived from NRP cells grown in growth medium (GM2), 3 h after re-plating in differentiation medium (DF), or after further incubation in differentiation medium containing 5 ng/ml TGFß1 for the indicated time (h). **(c)** Caspase-3 activity in TGFß1 treated NRP-152 cells. DEVD-pNA cleavage was measured in cytosolic extracts of differentiated NRP cells treated with 5 ng/ml TGFß1 for the indicated time (h) as described in the Materials and Methods. Values were normalized to untreated, differentiated cells (n=4). Error bars correspond to the standard error of the mean. **(d)** Immunoblot of PARP cleavage. Nuclear extracts from differentiated NRP cells treated with 5 ng/ml TGFß1 for the indicated time (h) (+), or left untreated (-), were probed with an anti-PARP antibody. The positions of the intact (PARP) and the amino-terminal cleavage product (cleaved) are indicated. **(e)** Immunoblot of $FLIP_L$ protein levels. Cytoplasmic extracts from differentiated NRP cells treated with TGFß1 as in **(d)** were immunoblotted with an anti-FLIP antibody. The positions of the full sized protein ($FLIP_L$) and the 43 kD amino-terminal cleavage product (cleaved) are indicated. The lane labeled "Control" corresponds to lysate from HEK293T cells transfected with a plasmid encoding $FLIP_L$.

Figure 2 Characterization of stable $FLIP_S$ transfectants (set 1). **(a)** TGFß1 induced apoptosis of $FLIP_S$ transfectants. Cultures were shifted to differentiation media, treated with 5 ng/ml TGFß1 and apoptotic (floating) cells counted after 72 h (n=4). Error bars correspond to the standard error of the mean. Bars correspond to the average apoptosis of parental NRP cell line (P), a clone transfected with the vector control (V1), and stable $FLIP_S$ transfected clones (numbered) with varying levels of expression (see **(b)**). **(b)** $FLIP_S$ and control transfectants described in **(a)** were grown in GM2 and protein extracts were immunoblotted with the anti-HA (upper panel), anti-FLIP (middle panel) or anti-actin (lower panel) antibodies. **(c)** Fragmentation of chromosomal DNA following TGFß1 treatment of differentiated NRP transfectants. Similar to Figure 1b; clones were treated with 5 ng/ml TGFß1 for 48 h. Lanes labeled as in **(a)** and **(b)**.

Figure 3 Caspase-3 activity of NRP transfectants (set 1). Cultures were differentiated, treated with 5 ng/ml TGFß1 and portions harvested at either 36 h to assay for caspase activity **(b-d)** or at 72 h to quantitate apoptosis **(a)**. **(a)** Apoptosis of $FLIP_S$ transfectants and controls (methods and labeling similar to Figure 2a). **(b)** Caspase-3 enzymatic activity of $FLIP_S$ transfectants and controls was determined and plotted as in Figure 1c (n=3). Samples labeled as in **(a)**. **(c)** Caspase-3 cleavage in $FLIP_S$ transfectants and controls. Cytoplasmic extracts from differentiated cultures (labeled as in **(a))** treated with 5 ng/ml TGFß1 for 36 h (+), or left untreated (-), were immunoblotted with an anti-caspase-3 antibody. The positions of the intact (Casp3) and the amino-terminal cleavage product (p17) are indicated. **(d)** PARP cleavage in $FLIP_S$ transfectants and controls. Nuclear extracts of differentiated cultures treated as in **(c)** were immunoblotted with an anti-PARP antibody. The position of the 117 kD intact PARP and the 84 kD cleavage product (cleaved) are indicated.

Figure 4 Characterization of $FLIP_S$ transfectants (set 2). **(a-b)** TGFß1 induced apoptosis of $FLIP_S$ transfectants. Additional stable $FLIP_S$ transfected NRP cultures were analyzed as in Figure 2a-b. Minor low mobility bands in the third panel of (b) correspond to the 43 kD cleaved form of $FLIP_L$, as seen in the control lane of Figure 1e. **(c)** Caspase-3 enzymatic activity of $FLIP_S$ transfectants and controls was determined and plotted as in Figure 3b (n=3). **(d)** PARP cleavage in $FLIP_S$ transfectants and controls was determined as in Figure 3d.

Figure 5 Rat Fas-Fc blocks FasL, but not TGFß1, induced cell death. **(a)** Anti-HA immunoblot of 1 µl purified HA tagged Fc (lane 1) and 1 µl Ha tagged rat Fas-Fc (lane 2) proteins. **(b)** Jurkat cell killing by mFasL is blocked by rFas-Fc. Jurkat cells were treated with diluent (solid bars), 200 pg/ml (diagonal striped bars), or 80 pg/ml (checkered bars) mFasL in the presence of diluent or the indicated amounts of Fc or rFas-Fc. After 18 h, WST-1 conversion to formazan was measured as described in Materials and Methods and normalized to untreated control Jurkat cells (n=4). Error bars correspond to the standard error of the mean. **(c)** NRP killing by mFasL is blocked by rFas-Fc, but killing by TGFß1 is not. NRP cells were differentiated and then treated with diluent (solid bars), 1 ng/ml (diagonal striped bars) or 5 ng/ml (checkered bars) TGFß1, or 2 ng/ml mFasL (horizontal striped bars) in the presence of diluent or the indicated amounts of Fc or Fas-Fc. After 72 h, WST-1 conversion to formazan was measured and plotted as in **(b)** (n=4). **(d)** NRP cell killing by TGFß1 is not blocked by high doses of rFas-Fc. NRP cells were differentiated and then either treated with 1 ng/ml TGFß1 or left untreated, in the presence of diluent (none) or the indicated amounts of Fc or Fas-Fc. After 72 h apoptotic (floating) cells were counted and the data plotted as in Figure 1a (n=3).

Figure 6 TRAIL R-Fc blocks TRAIL, not TGFß, induced cell death. **(a)** Jurkat cell killing by TRAIL is blocked by DR4-Fc. Jurkat cells were pre-treated with diluent (solid bars), or 250 ng/ml DR4-Fc (diagonal striped bars) for 3 h, followed by

human TRAIL at the indicated concentrations. After 18 h, WST-1 conversion was measured and plotted as in Figure 5b (n=4). **(b)** Jurkat cell killing by TRAIL is blocked by DR5-Fc. Similar to **(a)**, except DR5-Fc was used. **(c)** NRP cells are killed by mTRAIL. NRP cells were treated with the indicated concentration of mouse TRAIL. After 72 h, WST-1 conversion was measured as in Figure 5b (n=4). **(d)** NRP cell killing by TGFß1 is not blocked by DR4-Fc. NRP cells were pre-treated for 3 h with diluent (solid bars), or 250 ng/ml DR4-Fc (diagonal striped bars) and then treated with the indicated concentration of TGFß1. After 72 h, WST-1 conversion was measured as in Figure 5b (n=4). **(e)** NRP cell killing by TGFß1 is not blocked by DR5-Fc. Similar to **(d)**, except DR5-Fc was used. **(f)** NRP cell killing by TGFß1 is not blocked by the combination of DR4-Fc and DR5-Fc. Similar to **(d)**, except that a combination of DR4-Fc and DR5-Fc (each at 250 ng/ml) was used.

Figure 7 Insulin increases $FLIP_L$ levels in differentiating NRP-152 cells and blocks apoptosis. **(a)** Insulin blocks TGFß1 induced apoptosis. NRP cells were differentiated for 6 h in the presence of diluent (none), EGF or insulin (at the concentrations used in GM2) and then treated with 5 ng/ml TGFß1 (striped bars) or diluent (solid bars). After 72 h apoptotic (floating) cells were counted and the data plotted as in Figure 2a (n=3). **(b)** EGF and insulin differentially induce $FLIP_L$ expression. NRP cells were differentiated for 6 h in either the absence or presence of insulin or EGF and appropriate extracts were immunoblotted for $FLIP_L$, PARP and actin. Representative sample of 3 separate experiments. **(c-d)** Effects of EGF and insulin on $FLIP_L$ expression and PARP cleavage. NRP cells were differentiated for 6 h in either the absence or presence of insulin or EGF and then either left untreated or treated with 5 ng/ml TGFß1 for 24 or 48 h, all as indicated. Appropriate extracts were immunoblotted as in **(b)**. Representative samples of three separate experiments.

Nastiuk, et al. Figure 1

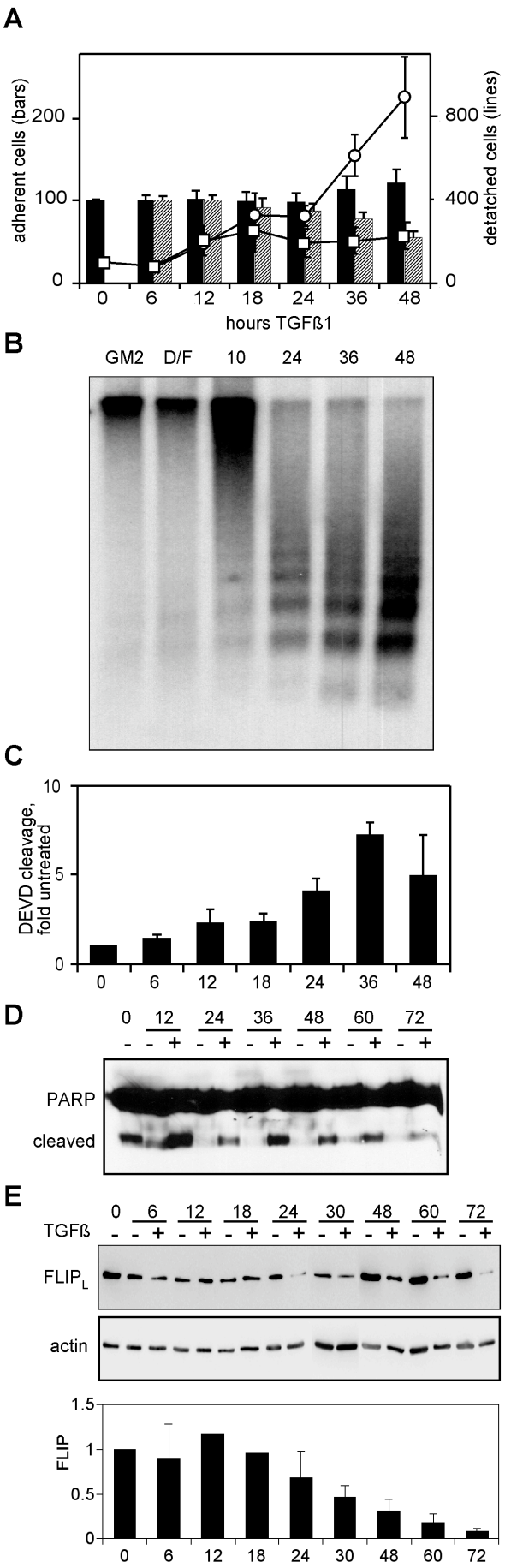

Nastiuk, et al. Figure 2

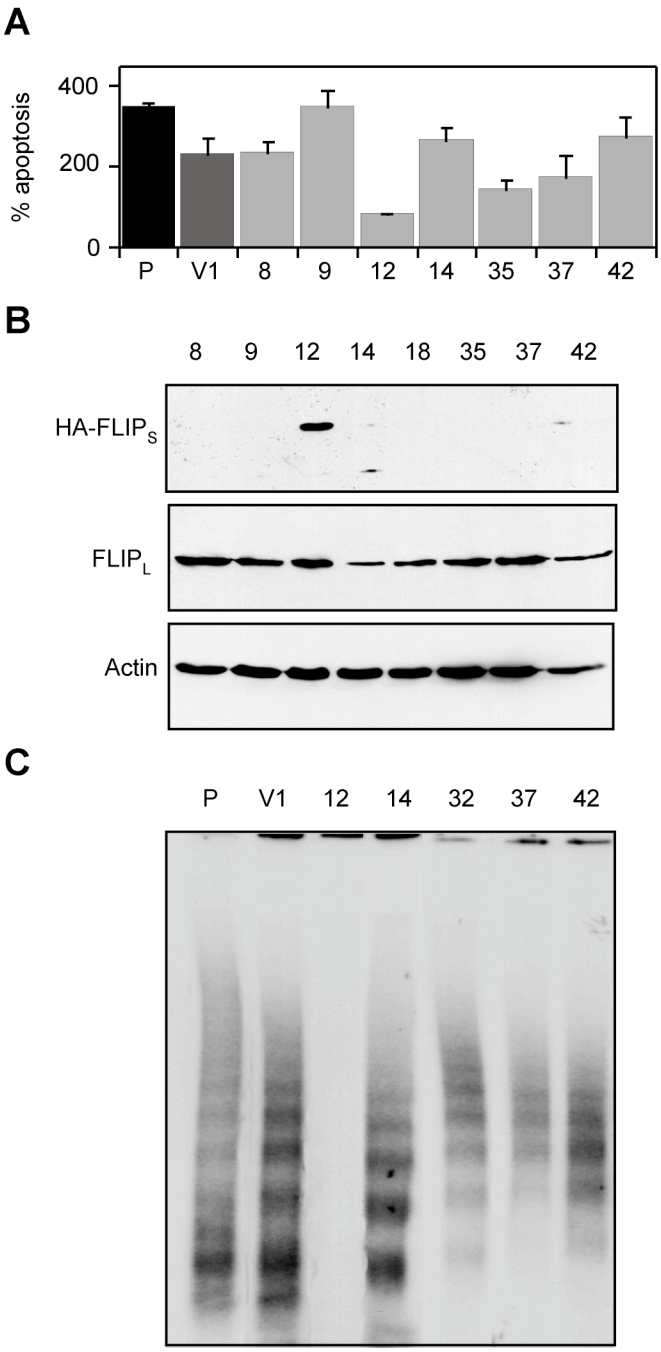

Nastiuk et al., Figure 3

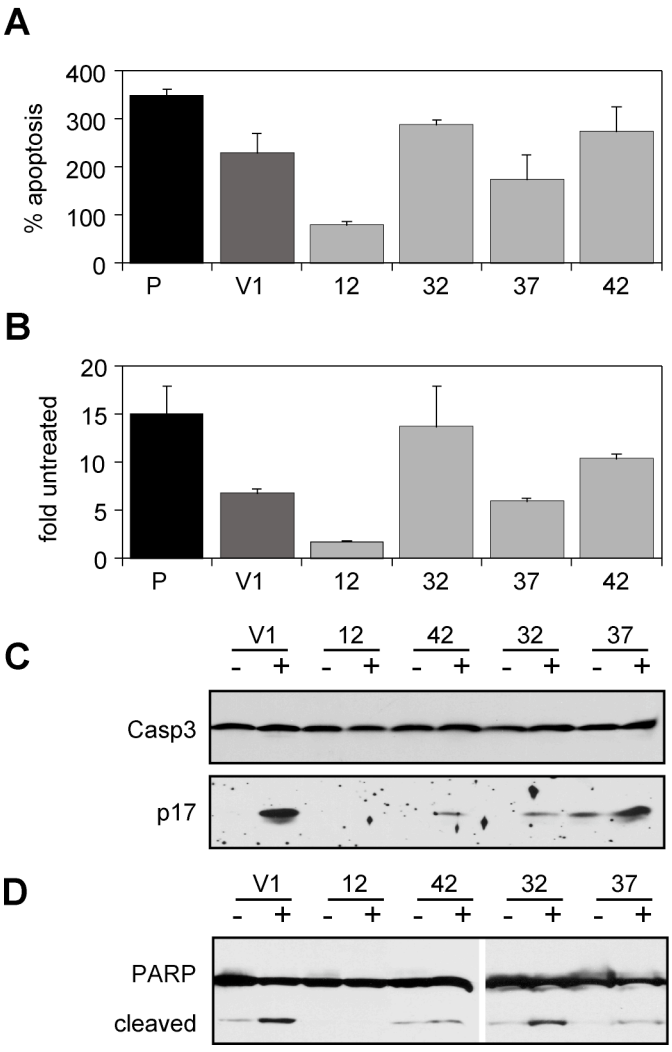

Nastiuk, et al, Figure 4

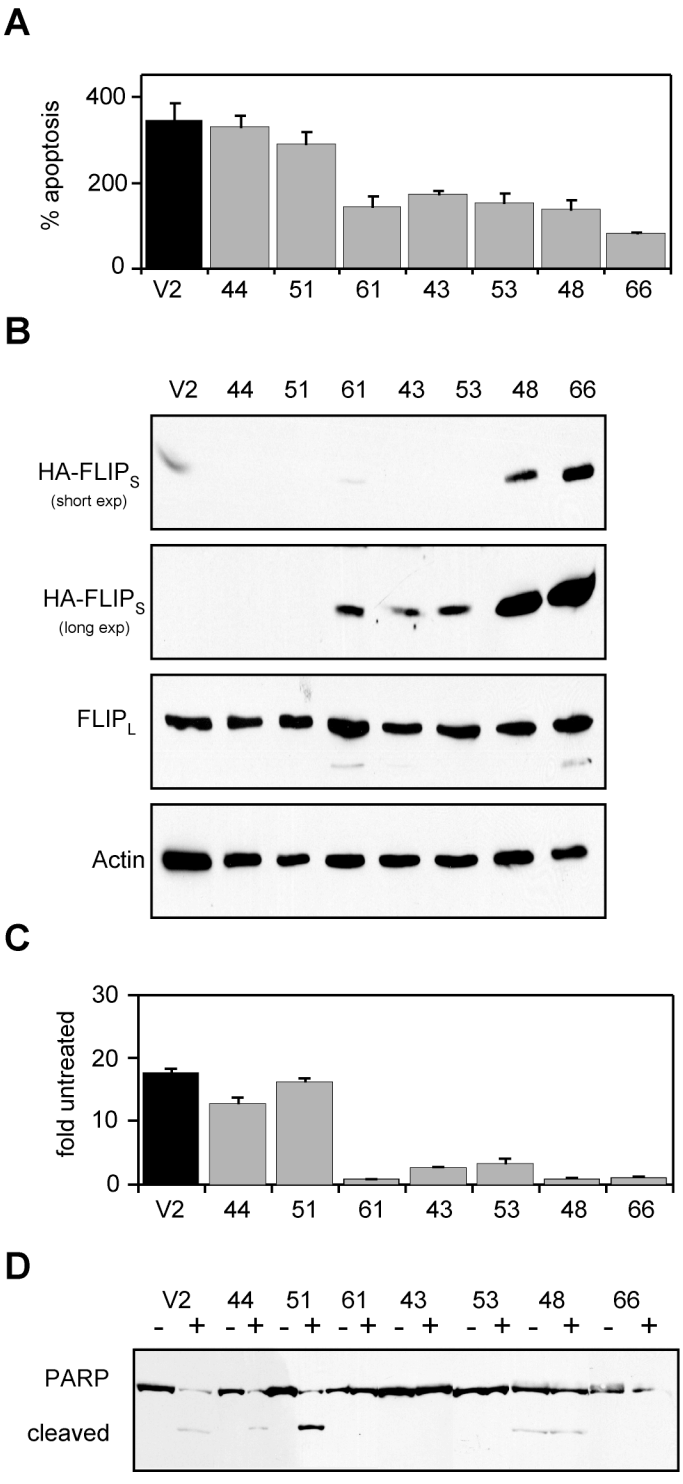

Nastiuk, et al., Figure 5

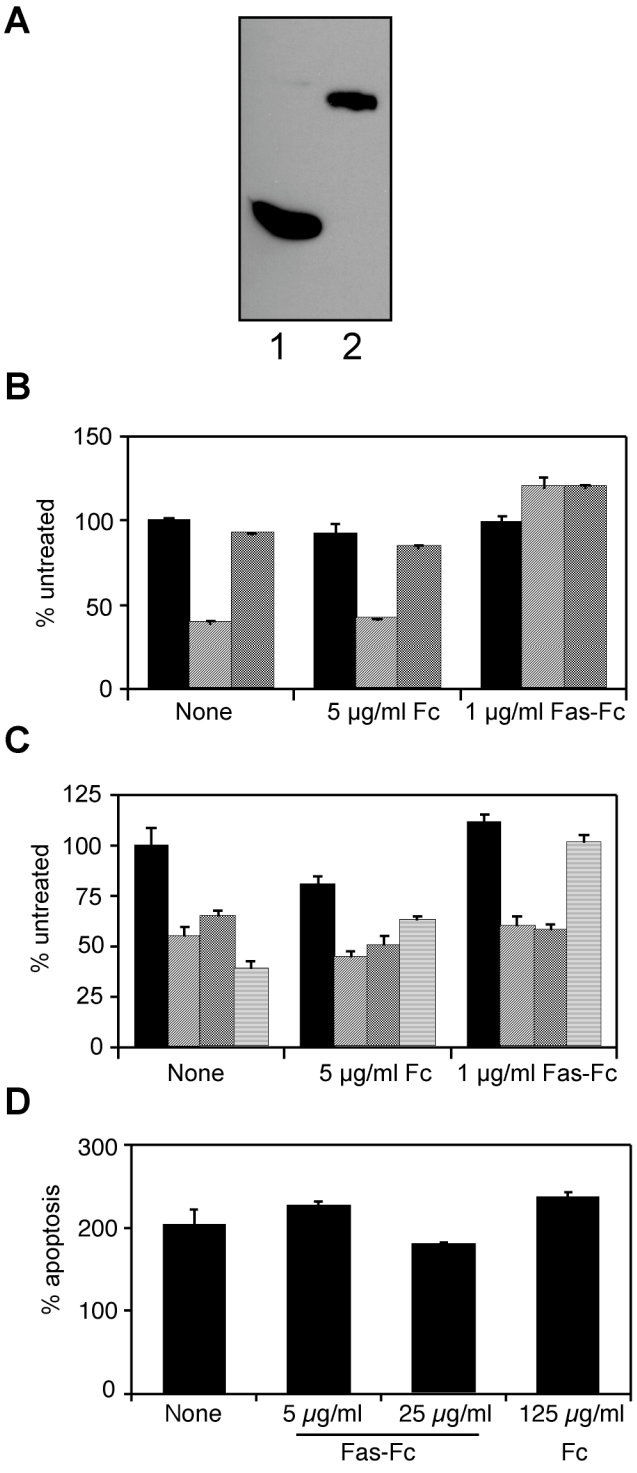

Nastiuk, et al., Figure 6

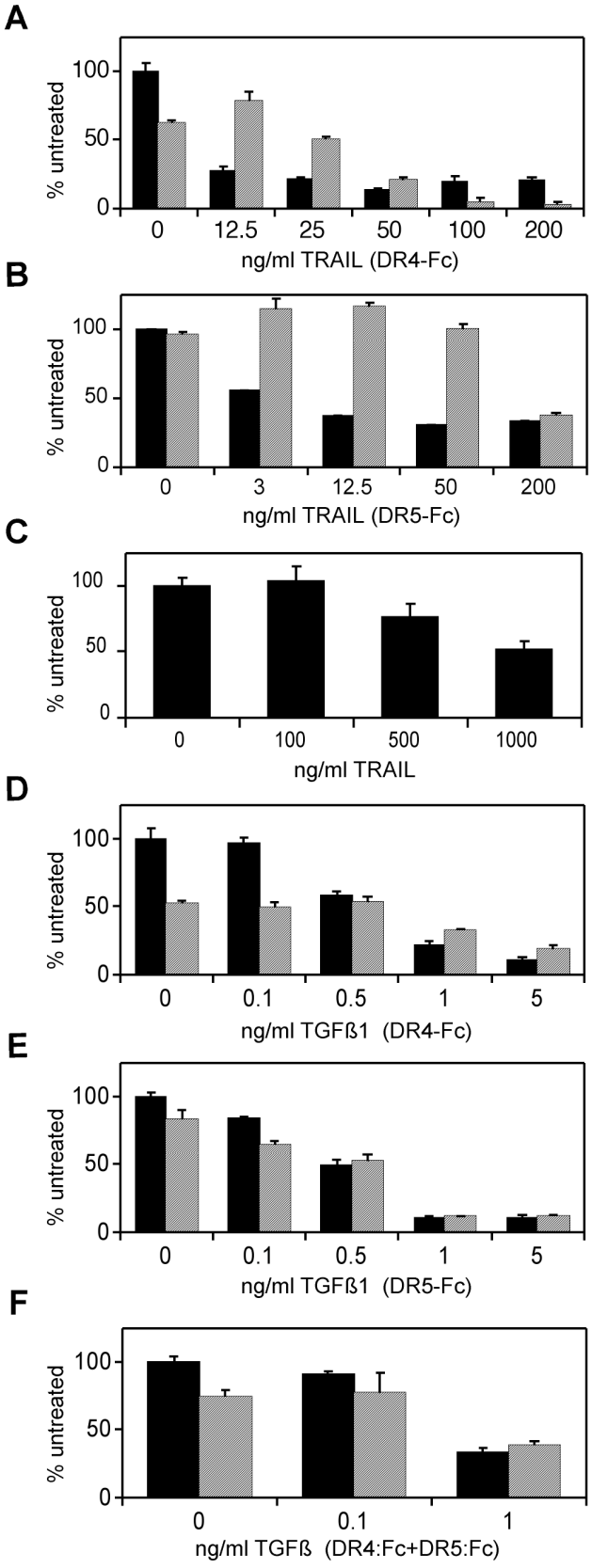

Nastiuk et al., Figure 7

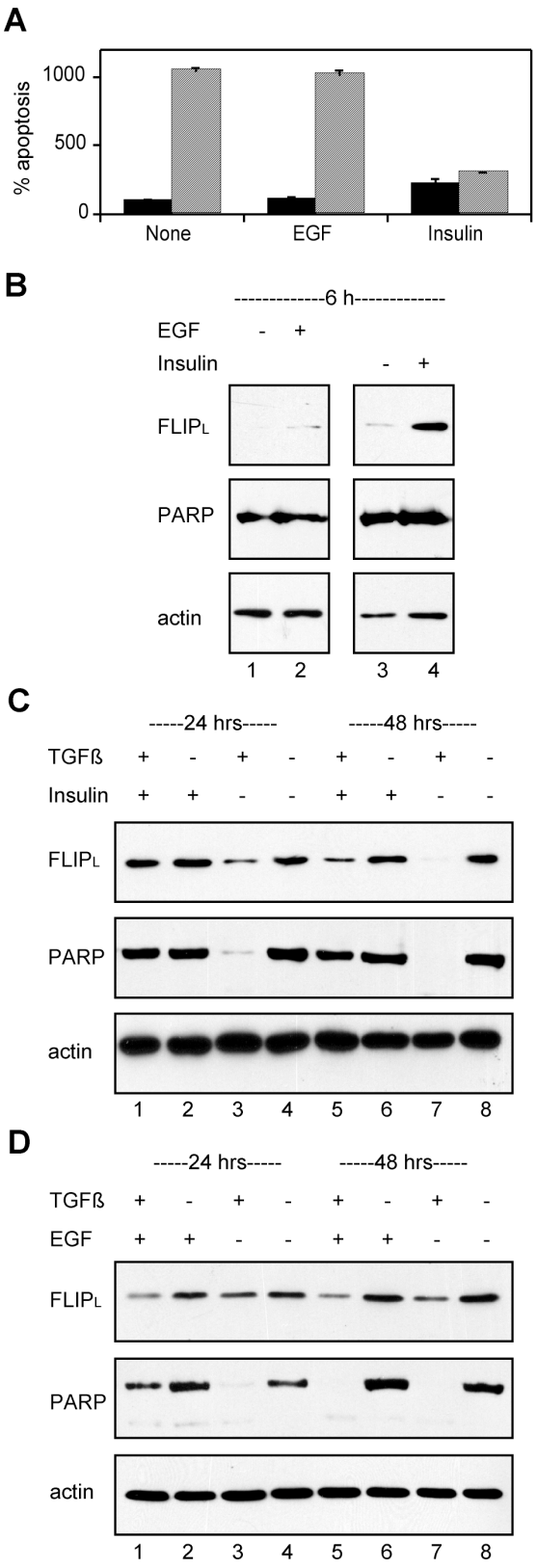

In vivo MRI volumetric measurement of prostate regression and growth in mice

Kent L. Nastiuk[1], Hui Liu[2], Mark Hamamura[2], L. Tugan Muftuler[2], Orhan Nalcioglu[2,4], and John J. Krolewski[1,3,*]

[1]Department of Pathology and Laboratory Medicine
[2]Center for Functional Onco-Imaging
[3]Chao Family Comprehensive Cancer Center
[4]Departments of Radiology, Physics, and Electrical Engineering
University of California, IRVINE
Irvine, CA 92697, USA

***Correspondence to:**
John Krolewski, Department of Pathology and Laboratory Medicine, School of Medicine, UC Irvine, Medical Sciences I D450, Irvine, CA 92697-4800
E-mail: jkrolews@uci.edu; Phone: 949-824-4089; Fax: 949-824-2160

Running Title: MRI measurement of prostate volume
Key Words: lobes, CHESS, DHT, castration, fat, imaging
Grant sponsor: CDMRP; grant number PC030937.

ABSTRACT

Background. Temporal monitoring of mouse prostate regression requires multiple animals and examination of histological sections due to the intercalated anatomical localization of the gland.
Results. High field (7T) MRI provides high resolution (117µm x 117µm in plane), highly reproducible images of the normal mouse prostate. Despite long imaging times, animals can be repeatedly imaged to establish reliability of volume measurements. Prostate volume declines following castration and subsequently returns to normal size with androgen administration in the same animal. A chemical shift-selective (CHESS) pulse was used to suppress fat content in the images and allowed discrimination of the dorsal lateral lobes of the prostate (DLP) from the ventral lobes (VP). Castration results in a 40% reduction in the volume of the DLP and a 75% reduction in the volume of the VP.
Methods. T2-weighted MRI was performed on normal C57Bl mice. Fat signal was suppressed to avoid signal contamination and enhance discrimination. Individual mice were repeatedly imaged over a period of many weeks.
Conclusions. MRI assessment of changes in the volume of the mouse prostate is very accurate and reproducible. The volume of individual lobes of the prostate can be measured, and monitoring of the same mouse over time during the course of treatment is possible.

INTRODUCTION

Androgens regulate the growth of both normal and neoplastic prostate. Thus, for almost fifty years the principal treatment for advanced stage prostate cancer has been androgen ablation therapy by orchiectomy or, more recently, pharmacological treatment with anti-androgens or gonadotropin inhibitors. While most such prostate cancers initially regress, they eventually become independent of androgens for growth and metastasize fatally. Mouse models of prostate cancer may prove very useful in dissecting the signaling pathways important for both progression to cancer and inhibition of tumor cell growth (1). As in humans, androgens promote mitosis and differentiation of rodent prostate ductal epithelium, and further, appear to inhibit apoptosis of the differentiated cells (Isaacs, 1984). After androgen ablation, the balance between mitosis and apoptosis is disrupted, and the prostate undergoes a wave of cell death resulting in the involution of the gland (2). However, in mice assessing the extent of growth of the prostate and particularly its regression due to therapeutic intervention or castration is quite difficult due to the location, small size and interdigitated anatomy of the prostate gland in situ.

The mouse prostate is located centrally in the abdomen and so is inaccessible to external measurement as a xenograft would be. A particularly large tumor, such as those that develop in TRAMP mice, would be detectible only at late stage. Regression of smaller tumors or the normal prostate due to castration, chemotherapeutics, chemoprevention, or failure of early stage prostate cancers to progress is normally only detectable by histological examination following sacrifice of the animal (3).

MR imaging of the mouse prostate allows for longitudinal studies assessing volume changes in an individual mouse prostate over time. To be most useful, the MRI should have a very high resolution, since the mouse prostate is normally only 20 mm^3 and it should allow successive monitoring of the same mouse. Xu et al (4) successfully imaged a cohort of xenograft bearing mice on two separate occasions using a commercial 1.5T instrument to visualize multiple mice simultaneously, but the resulting resolution was only 0.39 mm^3. Hsu et al (5) followed tumor development in TRAMP mice

with up to four imaging sessions in a 7T MRI with a resolution of 0.175 mm^3 and a number of other investigators have imaged the TRAMP mouse prostate in situ on a single occasion at higher resolutions (6,7). The effect of a chemopreventive drugs on the volume of the TRAMP mouse prostate was assessed at a single timepoint by MRI (8,9). The effect of castration on the volume of tumors in TRAMP mice was monitored in the same mouse up to four times over many months (10) but again the resolution was only 0.175 mm^3. Instead of assessing tumor volume, a single 2-D image was used to examine the effects of deleting the tumor suppressor genes PTEN and p53 on prostate cancer development by increased cross-sectional size in the mouse prostate (11,12). Fricke (13) recently reported using a 7T MRI 3-D imaging procedure to measure prostate volume in normal and knock-out animals at a high resolution (0.005 mm^3) and suggest that longitudinal studies would be possible.

We have improved both the reproducibility, accuracy, and resolution of prostate volume determination by MRI and employed this methodology to resolve two major lobes of the gland. Using this technique, we have monitored the castration-induced regression and androgen-induced regrowth of the normal prostate gland in individual animals with up to ten imaging sessions over a five weeks.

MATERIALS AND METHODS

Animals

Male C57BL6 mice were purchased from the NCI or Charles River Labs. All were retired breeders and more than one year old and. Mice were housed individually in the UCI animal facility and all procedures were in accordance with institutional guidelines. The animals were anesthetized with a combination of Xylazine and Ketamine (13 mg/kg and 87 mg/kg, respectively) and then castrated via scrotal incision. Each testical, vas deferens, and the accompanying fat pad was removed and the blood vessels and vas deferens ligated. The incision was closed with surgical silk rather than would clips for compatibility with MRI imaging. Androgen was replaced using 5 mg/kg 5-alpha-androstan-17-beta-ol-3-one (dihydrotestosterone, DHT, Sigma) in corn oil injected sub-cutaneously daily. For imaging, mice were anesthetized as above, and positioned inside the instrument. Anesthesia was maintained using 1% Isoflurane, 99% oxygen delivered via a nose cone surrounding the mouse's head while inside the magnet, for the duration of the imaging.

MRI

Animals were placed on a removable stage and insulated for warmth and held in position by wrapping in a piece of paper towel surrounded by plastic wrap. They were then positioned inside a shielded 8-leg highpass birdcage coil with 65mm diameter, constructed in-house, which was used for RF pulse transmission and signal reception. Experiments were performed on a MRRS (MR Research Systems Ltd., Surrey, UK) console interfaced to a 7T Oxford 300/150 horizontal bore magnet with an inner bore size of 150 mm (Oxford Instruments Limited. UK). The system is equipped with an actively shielded gradient coil (Model BFG-150/90-S, Resonance Research Inc, Billerica, MA) with a maximum gradient strength of 750 mT/m, 100µs rise time and inner diameter of 90mm. The gradients are driven by Techron series 7700 linear gradient amplifiers, with a maximum slew rate of 150 T/m/s.

A set of scout proton spin-echo images in the axial orientation (TR/TE = 1080ms/23ms , 25 slices, slice thickness =0.5mm, image matrix size=128 x 128 FOV=35mm^2), were obtained to accurately localize the position of the mouse prostate. Then a 2D interleaved multi-echo spin-echo sequence (TR/TE=4500msec/20ms, 32 slices, slice thickness = 0.3 mm with no separation, image matrix size=256 x 256, field of view (FOV)=30mm x 30mm, NEX= 8 averages) was used to produce images for volume determination.

Subsequently, imaging was performed incorporating a chemical suppression sequence (CHESS) to suppress the signal from the abdominal fat. After the scout images were obtained, spectroscopy was used to identify the resonant frequency of the lipid-derived protons (typically 950-1000Hz). A Gaussian 240Hz pulse was used for CHESS fat suppression using the lipid resonance frequency and a pulse duration of 1000 µs. A 2D interleaved CHESS Spin-echo with fat suppression sequence (TR/TE=4500msec/25ms, 32 slices, slice thickness = 0.2mm with no separation, image matrix size=256x256, FOV=30 mm x 30mm, NEX = 8 averages) was used to acquire the fat-suppressed MR images of mouse prostate.

Volume determination

Each series of 32 image slices was analyzed using NIH ImageJ (http://rsb.info.nih.gov/ij/). These were assembled as a stack and magnified 4-fold in the x and y orientation for more accurate boundary drawing. The edges of the prostate (or lobes) were delineated by tracing, and the number of bounded pixels in the slice was computed. The total number of pixels from each slice containing prostate was summed, divided by the magnification factor, and finally multiplied by the voxel size to give the prostate volume. The voxel size is the

volume represented by one pixel in the MRI. It is the image resolution, 117 µm x 117 µm (computed by dividing the FOV, 30 mm^2, by the number of points in the image matrix, 256 x 256) and multiplying by the slice thickness. The voxel size for these studies is 0.0041 mm^3, and for the CHESS images it is 0.0027 mm^3. Volumes were determined twice for each image session and the mean presented. Multiple MR images were captured of most mice before treatment (normals), and the mean of the volumes and the accompanying standard error are presented.

RESULTS

Imaging of the normal prostate

In order to determine the optimal parameters for imaging the mouse prostate *in vivo*, mice were examined using T1- and T2-weighted images (data not shown, DNS). T2-weighted images were superior due to less fat interference. The echo time of the T2-images also affected image quality, and among 20, 40, and 80 msec echo times, 20 msec resulted in the best differentiation of the prostate from the surrounding tissue (DNS). Finally, we determined that averaging 8 image sets gave an adequate image signal to noise ratio while limiting the imaging time to 2.5h, or 3.5h including the initial imaging necessary to position the mouse and shim the magnet. Maintaining anesthesia using injectables (Xylazine/Ketamine) proved difficult due to decreased respiration and body temperature, and so a combination of initial anesthesia with injectables and maintenance of anesthesia using Isoflurane/oxygen inhalation inside the magnet gave 90-100% survival. Longer total time under anesthesia resulted in increased incidence of respiratory failure and loss of the animals, which we need to avoid in order to image the same animal over multiple sessions. Finally, images were collected from two test mice and the identification of each organ on the MRI was confirmed by gross examination (DNS).

Prostate volumes were measured from mature mice. The reproducibility of the measurements over multiple imaging sessions was very good. Figure 1 shows image slices of the prostate from one mouse (batch 3, mouse 3 (b3m3)) imaged on three separate days. One slice containing the prostate from each session is show in Figure 1 (panels A1, A2, and A3). The circumference of the prostate was outlined on each slice (typically 10-20 slices total) which contained identifiable prostate (illustrated in panels A1', A2', and A3'). The number of pixels in each bounded prostate slice was then added and multiplied by the voxel size, 0.0041 mm^3, to give the volume of the prostate, 22.1 mm^3+/- 1.0 mm^3 for mouse b2m3. Additional examples of images from other normal mature mice in Figure 1, panels B, C, and D show similar prostate size when the circumscribed (Figure 1, panels B', C', and D') areas are totaled. The volume of seven individual normal mature mouse prostates is shown in Figure 1F, where the first three mice (b2m3, b3m2, and b3m3) were imaged three times each (n=3), the following two mice (b4m1, b4m2) imaged a single time, and the final two mice (b5m1, b5m2) imaged twice. We find the overall average volume is 23.80, +/- 0.98 mm^3 for all mice, and that a single imaging session is sufficient estimate of the prostate volume.

Imaging regression of the prostate following castration

Three of these mice were castrated following MRI assessment of normal prostate volume, and reduction of the prostate volume was assessed over the following weeks. Figure 2 shows the prostate image which contains the maximum cross-sectional area for a series of imaging sessions performed on one mouse one (A), three (B), eight (C), and ten (D) days after castration. The prostates declined almost 75% in volume following castration (Figure 2E), to 6.04 +/- 0.61 mm^3.

Figure 2 also illustrates two problems with following the regression of the mouse prostate. The fat surrounding the prostate produces an intense signal which appears to 'shift' into the prostate and, as the prostate regresses, its composition (of water, fat, prostatic fluid, or other constituents) changes resulting in a reduced signal to noise ratio, and hence differentiation of the prostate from surrounding tissues,
in the MR images.

Optimizing MRI imaging reveals prostate lobes

The MRI signal shift due to fat is illustrated in Figure 3. The white arrow in Figure 3A indicates a region of fat signal shift of several millimeters, within the muscle. The intense fat signal shift down and to the left leaves a dark area corresponding to the region vacated by the shifting fat signal. In the magnified image (panel A') of the central portion of Figure 3A the black arrows point to a void on the left resulting from the fat signal shift, and on the right to a hyperintense region where the fat signal has shifted into the area of the prostate.

Fat signal can be greatly reduced by selectively suppressing fat protons prior to acquiring the water proton signal, using a chemical shift selective imaging sequence (CHESS). The frequency of fat proton emission is determined during pilot imaging, and a presaturation pulse is applied prior to slice image acquisition. Figure 3B shows the image slice of a normal mouse acquired using CHESS. The intense

abdominal fat (labeled F in Figure 3A') and other fat signals have been eliminated. The magnified image in Figure 3B' shows that the borders of the prostate are well delineated. A surprising result of the CHESS imaging is the greater signal intensity in the ventral lobe relative to the dorsal lateral region (VP versus DLP in Figure 3B'). This increased relative intensity may be due to higher water content of the prostatic fluids in the more numerous secretory ducts of the ventral lobe.

We then used CHESS imaging to determine the volume of the lobes of the normal mouse prostate. At the same time, we increased the accuracy of our volumetric determinations by reducing the slice thickness to 200μm, resulting in a voxel size of 0.00274 mm^3. The solid bars in Figure 3C show the volumes of the VPs derived from four normal mice (19.04 +/- 1.60 g). The striped bars show the DLP, whose average volume is 12.39 +/- 0.75 g. While Figure 1 reveals good reproducibility and inter-animal agreement for total prostate volume, examination of the CHESS images shows that those values underestimate the total volume (VP + DLP) of the prostate (23.80 g versus 31.42 g).

Regression and regrowth of individual lobes of the mouse prostate

The ventral lobe of the rodent prostate regresses more than the dorsal or lateral lobes. In rats, the wet weight of the ventral lobe is reduced 75% within 10 days of castration, while the dorsal and lateral lobes are only reduced 50% (Banjaree '95). Figure 4 shows a time course (similar to Figure 2) of CHESS images of a mouse prostate following castration (panels A-D) with the ventral prostate outlined in white and the dorsal in black (panels A'-D'). CHESS imaging greatly enhances the signal to noise in the images at the later time-points and the elimination of the fat signal overlap allows more accurate delineation of the boundaries of the lobes of the prostate. The volume of the ventral prostate is reduced over 10 days to 28% of starting volume (Figure 4E). The reduction in volume of the dorsal lateral prostate is smaller, to 61% of the starting volume (Figure 4F).

The prostate of a castrated animal will grow to pre-castrate size, and indeed larger ,if the animal is given androgens. Two weeks following castration, mice were given daily injections of DHT and the prostate was monitored by MRI. Figure 5, panels A-F show this regrowth over a two week period. The dorsal lateral lobes, outlined in black in panels A'-F', double in size after 9 days of treatment at which time growth is arrested (Figure 5G, squares). In contrast, the ventral lobe, outlined in white, returns to precastration size in the same period, but then continues to increase in size for the duration of the treatment (Figure 5G, circles).

DISCUSSION

We applied MR imaging to accurately quantitate the volume of the mouse prostate *in vivo*. We have optimized the MRI technology protocol in a variety of ways to significantly improve on previous applications of MRI to prostate imaging in the mouse. Specifically, we used a high-field magnet and a small coil in order to maximize the resolution. We also refined the anesthesia techniques that allowed us to image a mouse for 3.5 hours. Extended imaging time is necessary to produce the best quality images, by providing sufficient time to position the mouse at the focal point of the field, adjust (shim) the magnetic field, and capture eight averages of the image, improving the signal to noise ratio. We used a 256 x 256 matrix, a small (30mm) FOV, and very thin (200 μm) non-interleaved slices to obtain the smallest voxel size reported for mouse prostate imaging. Our protocol could accurately determine the volume of the normal prostate from a single MR image set, as evidenced by the observation that additional imaging sessions did not vary significantly. Thus, the approach described here allows for high quality imaging of the prostate without the need for repeated imaging sessions, thereby reducing the incidence of anesthesia-induced animal death. While our method was developed independently, it generates prostate volumes similar to those reported in the MRI studies of Fricke, et al. (13). Their reported volume for a C57Bl6 mouse prostate is 25.9 mm^3 from a single mouse prostate image set evaluated three times, while we report an average volume of 23.8 mm^3 from six different mice and 15 image sets. We were able to reduce our voxel size two fold relative to theirs (0.0027 versus 0.0051 mm^3). This enhanced resolution produces more accurate volume determinations.

The development of mice deficient for genes involved in apoptosis signaling has proved to be a fruitful means to identify key regulators of cancer development and progression in the rodent prostate (3). Similarly, understanding the genetic basis of androgen withdrawal induced regression will provide insights into the androgen-deprivation induced progression of prostate cancer. Measuring apoptosis and regression in mouse prostate is technically challenging. In contrast, the lobes of the rat prostate are larger and can therefore be much more readily physically dissected from surrounding tissues. Regression can be monitored by sacrificing the rats, recovering the prostate and weighing the individual lobes. This physical separation also allows the measurement of protein content, DNA content, and the appearance of low molecular weight DNA due to apoptosis. Two weeks following castration, the ventral and dorsal lobes lose 50% of their mass,

while the ventral lobes lose 75% (14). In the mouse we find a 75% loss of volume after the castration induced regression of whole prostate (Figure 2). When we used the improved resolution of the CHESS fat suppression technique to differentiate images of the lobes into the bright ventral portion and dorsolateral remainder, again we find that regression in the mouse closely parallels the rat, with a 75% reduction of the VP and a 50% reduction of the DLP (Figure 4).

Since physical isolation of the lobes of the mouse prostate is much more difficult than the rat (15), many investigators use histological techniques to measure apoptosis rather than measuring whole organ regression. Pyknotic cells or TUNEL labeled cells increase after castration in the rat prostate, but differences between castrated and normal prostate are very small (5 versus 30 per 100 acini) (16) and so a large number of sections must be examined for accurate assessment of differences. In the prostate, the appearance of cells which appear pyknotic and stain by TUNEL is also quite transitory, spanning a period of only four hours in the rat (17). For these reasons, studies examining castration-induced regression of the mouse prostate have yielded contradictory results for some important signaling pathways, particularly Fas. To measure the effects of Fas deletion on androgen withdrawal induced regression of the prostate, both the organ size and rate of apoptosis have been measured in Fas-deficient (lpr) mice. Two studies sacrificed groups of animals at intervals following castration and microdissected and weighed the prostates. Since accurate microdissection is technically challenging , it is perhaps not surprising that these groups reported contradictory results (18,19). Two reports also measured the incidence of apoptotic cells by either histological characteristics (19) or TUNEL staining (20) in castrated Fas deficient mice and report no difference between deficient and normal mice. However, small differences in apoptotic or proliferation rate accumulate over time to yield measurable changes in prostate volume (2). Thus, use of the MR imaging techniques described in this report might provide a more accurate method to revisit the role of Fas in androgen withdrawal induced apoptosis.

Our examination of the castration induced regression of the normal mouse prostate shows that we can track the reduction in total prostate volume (Figure 2) and that using CHESS to suppress fat signal, we can track the reduction of individual prostate lobes (Figure 4). We are also able to monitor the regrowth of the prostate after reversal of the androgen withdrawal induced increase in apoptosis by administering exogenous androgens (Figure 5). This MRI technique is sufficiently sensitive to detect even small changes in the size of the mouse prostate since monitoring of one animal repeatedly over time is more accurate than monitoring the mean of a group of animals sacrificed at intervals after castration or other treatment. An added benefit is to dramatically reduce the number of animals needed to measure the effect of any given manipulation.

CONCLUSIONS

We have optimized very high resolution imaging of the mouse prostate in living animals. Using these conditions, it is possible to repeatedly image a single mouse during the course of an investigation to monitor the effects of agents such as growth factors or chemotherapeutics on the rate of normal or tumor growth in the prostate. Using the CHESS technique, we were able to further discriminate the ventral from the dorsal and lateral lobes of the prostate, and monitor volume changes in each individually. This additional level of anatomic discrimination should be useful in monitoring lobe-specific tumor growth in mice.

ACKNOWLEDGEMENTS

This work was supported by a grant to J.J.K. from the DOD Prostate Cancer Research Program (PC030937), and by funds from the NIH (P30 CA062203) to O.N.

REFERENCES

1. Kasper S, Smith JA, Jr. Genetically modified mice and their use in developing therapeutic strategies for prostate cancer. J Urol 2004;172(1):12-19.
2. Denmeade SR, Lin XS, Isaacs JT. Role of programmed (apoptotic) cell death during the progression and therapy for prostate cancer. Prostate 1996;28:251-265.
3. Roy-Burman P, Wu H, Powell WC, Hagenkord J, Cohen MB. Genetically defined mouse models that mimic natural aspects of human prostate cancer development. Endocr Relat Cancer 2004;11(2):225-254.
4. Xu S, Gade TP, Matei C, Zakian K, Alfieri AA, Hu X, Holland EC, Soghomonian S, Tjuvajev J, Ballon D, Koutcher JA. In vivo multiple-mouse imaging at 1.5 T. Magn Reson Med 2003;49(3):551-557.

5. Hsu CX, Ross BD, Chrisp CE, Derrow SZ, Charles LG, Pienta KJ, Greenberg NM, Zeng Z, Sanda MG. Longitudinal cohort analysis of lethal prostate cancer progression in transgenic mice. J Urol 1998;160(4):1500-1505.
6. Shukla S, Maclennan GT, Marengo SR, Resnick MI, Gupta S. Constitutive activation of P I3 K-Akt and NF-kappaB during prostate cancer progression in autochthonous transgenic mouse model. Prostate 2005;64(3):224-239.
7. Song SK, Qu Z, Garabedian EM, Gordon JI, Milbrandt J, Ackerman JJ. Improved magnetic resonance imaging detection of prostate cancer in a transgenic mouse model. Cancer Res 2002;62(5):1555-1558.
8. Gupta S, Hastak K, Ahmad N, Lewin JS, Mukhtar H. Inhibition of prostate carcinogenesis in TRAMP mice by oral infusion of green tea polyphenols. Proc Natl Acad Sci U S A 2001;98(18):10350-10355.
9. Garcia GE, Wisniewski HG, Lucia MS, Arevalo N, Slaga TJ, Kraft SL, Strange R, Kumar AP. 2-Methoxyestradiol inhibits prostate tumor development in transgenic adenocarcinoma of mouse prostate: role of tumor necrosis factor-alpha-stimulated gene 6. Clin Cancer Res 2006;12(3 Pt 1):980-988.
10. Eng MH, Charles LG, Ross BD, Chrisp CE, Pienta KJ, Greenberg NM, Hsu CX, Sanda MG. Early castration reduces prostatic carcinogenesis in transgenic mice. Urology 1999;54(6):1112-1119.
11. Chen Z, Trotman LC, Shaffer D, Lin HK, Dotan ZA, Niki M, Koutcher JA, Scher HI, Ludwig T, Gerald W, Cordon-Cardo C, Pandolfi PP. Crucial role of p53-dependent cellular senescence in suppression of Pten-deficient tumorigenesis. Nature 2005;436(7051):725-730.
12. Trotman LC, Niki M, Dotan ZA, Koutcher JA, Di Cristofano A, Xiao A, Khoo AS, Roy-Burman P, Greenberg NM, Van Dyke T, Cordon-Cardo C, Pandolfi PP. Pten dose dictates cancer progression in the prostate. PLoS Biol 2003;1(3):E59.
13. Fricke ST, Rodriguez O, Vanmeter J, Dettin LE, Casimiro M, Chien CD, Newell T, Johnson K, Ileva L, Ojeifo J, Johnson MD, Albanese C. In vivo magnetic resonance volumetric and spectroscopic analysis of mouse prostate Cancer Models. Prostate 2006;66:708-717.
14. Banerjee PP, Banerjee S, Tilly KI, Tilly JL, Brown TR, Zirkin BR. Lobe-specific apoptotic cell death in rat prostate after androgen ablation by castration. Endocrinol 1995;136(10):4368-4376.
15. Suwa T, Nyska A, Haseman JK, Mahler JF, Maronpot RR. Spontaneous lesions in control B6C3F1 mice and recommended sectioning of male accessory sex organs. Toxicol Pathol 2002;30(2):228-234.
16. Hu Z, Ito T, Yuri K, Xie C, Ozawa H, Kawata M. In vivo time course of morphological changes and DNA degradation during the degeneration of castration-induced apoptotic prostate cells. Cell Tissue Res 1998;294(1):153-160.
17. Berges RR, Furuya Y, Remington L, English HF, Jacks T, Isaacs JT. Cell proliferation, DNA repair, and p53 function are not required for programmed death of prostatic glandular cells induced by androgen ablation. Proc Natl Acad Sci U S A 1993;90(19):8910-8914.
18. Suzuki A, Matsuzawa A, Iguchi T. Down regulation of Bcl-2 is the first step on Fas-mediated apoptosis of male reproductive tract. Oncogene 1996;13:31-37.
19. Sugihara A, Yamada N, Tsujimura T, Iwasaki T, Yamashita K, Takagi Y, Tsuji M, Terada N. Castration induces apoptosis in the male accessory sex organs of Fas- deficient lpr and Fas ligand-deficient gld mutant mice. In Vivo 2001;15(5):385-390.
20. de la Taille A, Chen MW, Shabsigh A, Bagiella E, Kiss A, Buttyan R. Fas antigen/CD-95 upegulation and activation during castration-induced regression of the rat ventral prostate gland. Prostate 1999;40:89-96.

FIGURE LEGENDS

Figure 1. MRI of normal mouse prostate. Prostates from year old C57BL6 mice (normal) were imaged. **A**: b3m3 images from three different days (**A1**, **A2**, **A3**). **B**: b3m2, **C**: b4m1, **D**: b2m3. Second column (**A1'-D'**) show the prostate outlined in white. Each image is the central 7.5 mm (64 X 64 pixel) portion of the complete MRI image (30 mm, 256 pixel square). **F**: Plot of prostate volumes for the indicated mice, in cubic millimeters. Error bars represent standard error of the mean of the prostate volume for each animal that was imaged multiple times (b4m2 and b4m2 were only imaged once).

Figure 2. MR image of prostate following castration. **A**: 1 day; **B**: 3 days; **C**: 8 days; and **D**: 10 days. The second column (**A'-D'**) shows the prostate outlined in white. Each image is the central 7.5 mm (64 X 64 pixel) portion of a complete MRI image (30 mm, 256 pixel square). **E**: Regression of the prostates of three individual mice. Square symbols represent the volume of the prostate of b2m3, circles represent b5m1, and triangles represent b5m2.

Figure 3. CHESS suppresses fat signal artifact and facilitates discrimination between ventral and dorsal-lateral lobes. **A:** T2- weighted MRI. **A'**: Magnification of the central 64 x 64 pixel square, indicated by the white box in **A**. White arrow in A and black arrows in **A'** illustrate the shift of the signal derived from fat. The location of the prostate (P), ureter (U) and abdominal fat (F) are indicated. **B**: T2- weighted image acquired using CHESS . **B'**: Magnification as in **A'**. White arrows indicate ventral prostate (VP) and dorsal-lateral prostate (DLP). **C**: Volume of the VP (solid bars) and DLP (striped bars) of normal mice determined using CHESS imaging.

Figure 4. MR-CHESS imaging of prostate involution. Prostate from year old C57BL6 mouse b6m1 following castration **A**: 1 day **B**: 3 days **C**: 8 days **D**: 10 days. Second column (**A'-D'**) show the ventral prostate outlined in white and the dorsal lateral prostate outlined in black. Each image is the central 7.5 mm square (64 X 64 pixel) portion of the complete MRI image (30 mm, 256 pixel square). **E**: Plot of prostate volume during regression of the ventral prostates of two individual mice. **F**: Plot of prostate volume during regression of the dorsal lateral prostate of two individual mice. Triangle symbols represent the volume of the prostate of b5m3 and circles are b6m1.

Figure 5. MR-CHESS imaging of prostate regrowth during androgen supplementation of castrated mice. Prostate from year old C57BL6 mouse b7m1 following castration and DHT treatment. **A**: day 0 (16 days following castration) **B**: 2 days DHT treatment **C**: 4 days DHT treatment **D**: 9 days DHT treatment. **E**: 12 days DHT treatment. **F**: 16 days DHT treatment. Second column (**A'-F'**) show the VP outlined in white and DLP outlined in black. Each image is the central 7.5 mm (64 X 64 pixel) portion of the complete MRI image (30 mm, 256 pixel square). **G**: Plot of prostate volume during regrowth of the ventral prostates of two individual mice. Triangle symbols represent the volume of the prostate of b5m2, circles represent the volume of the VP of b7m1 and squares represent the volume of the DLP of b7m1.

FIGURE 1

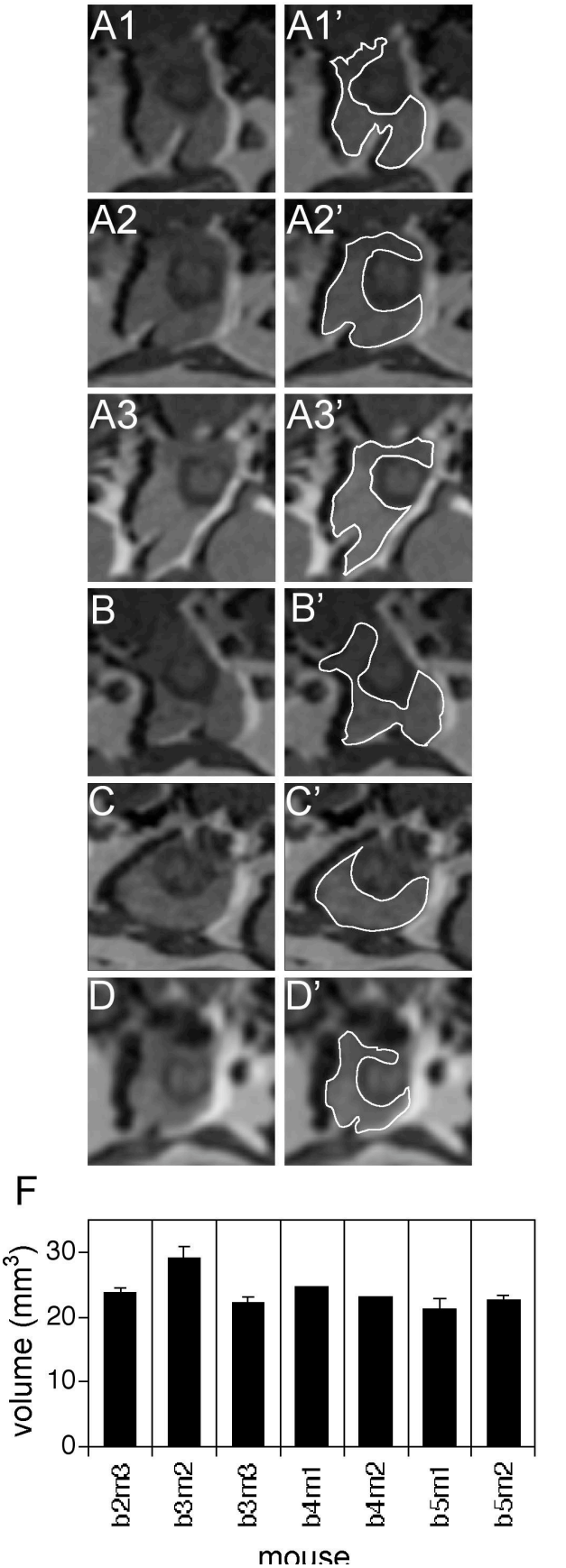

FIGURE 2

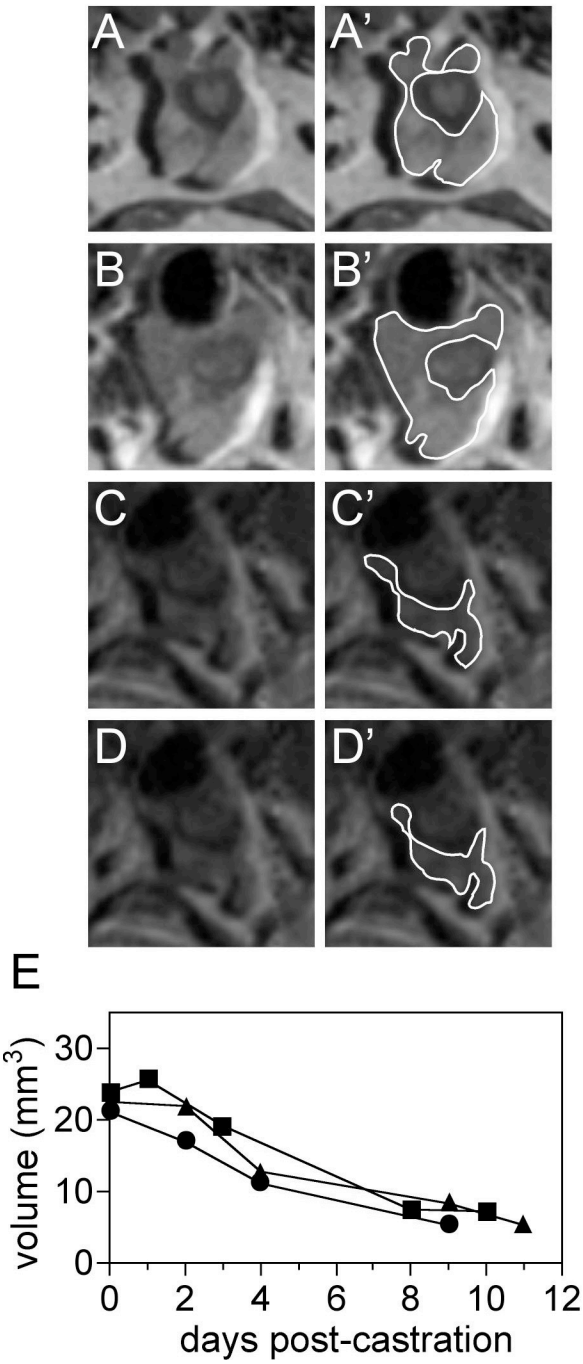

FIGURE 3

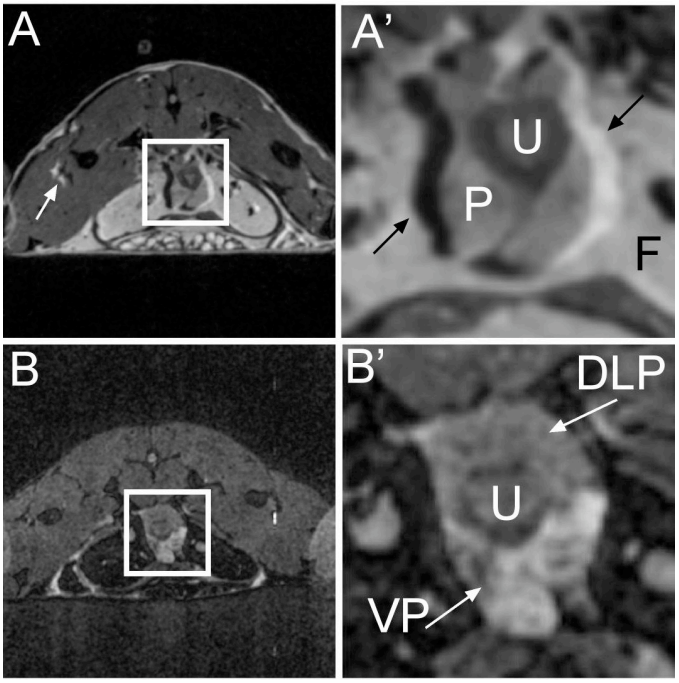

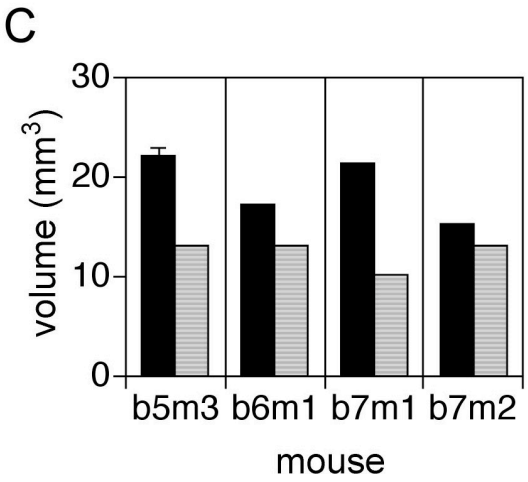

FIGURE 4

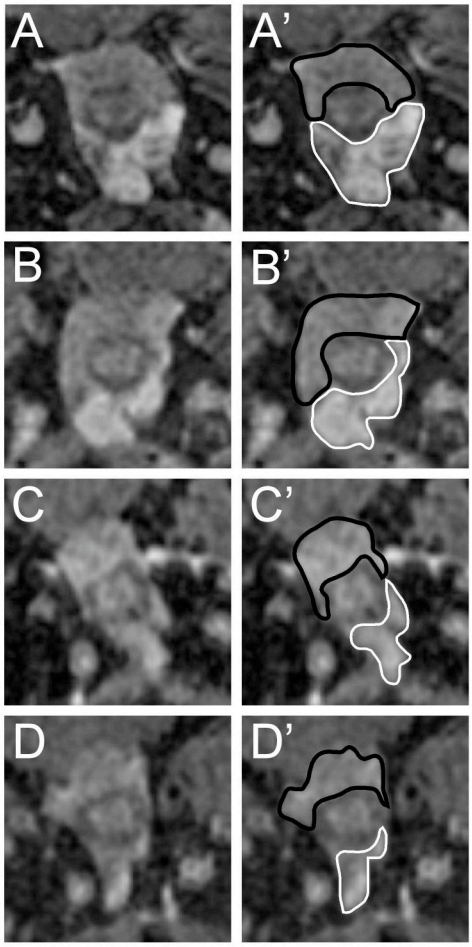

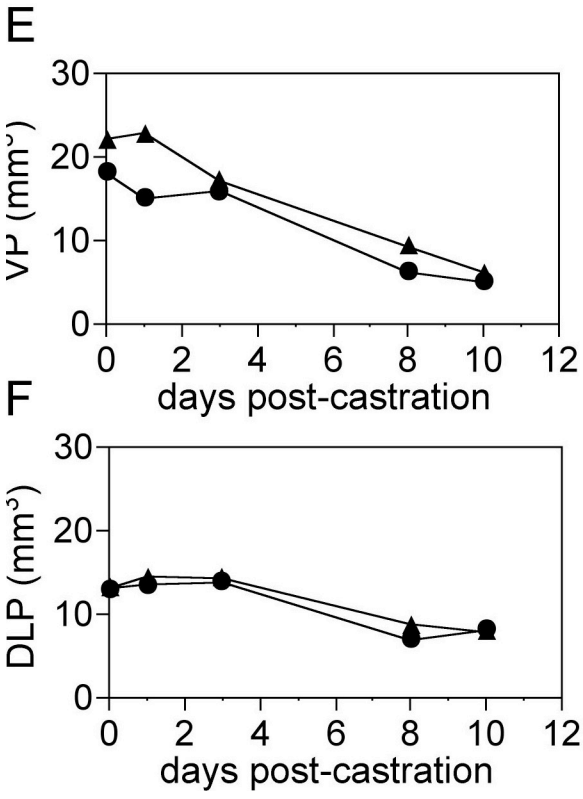

FIGURE 5

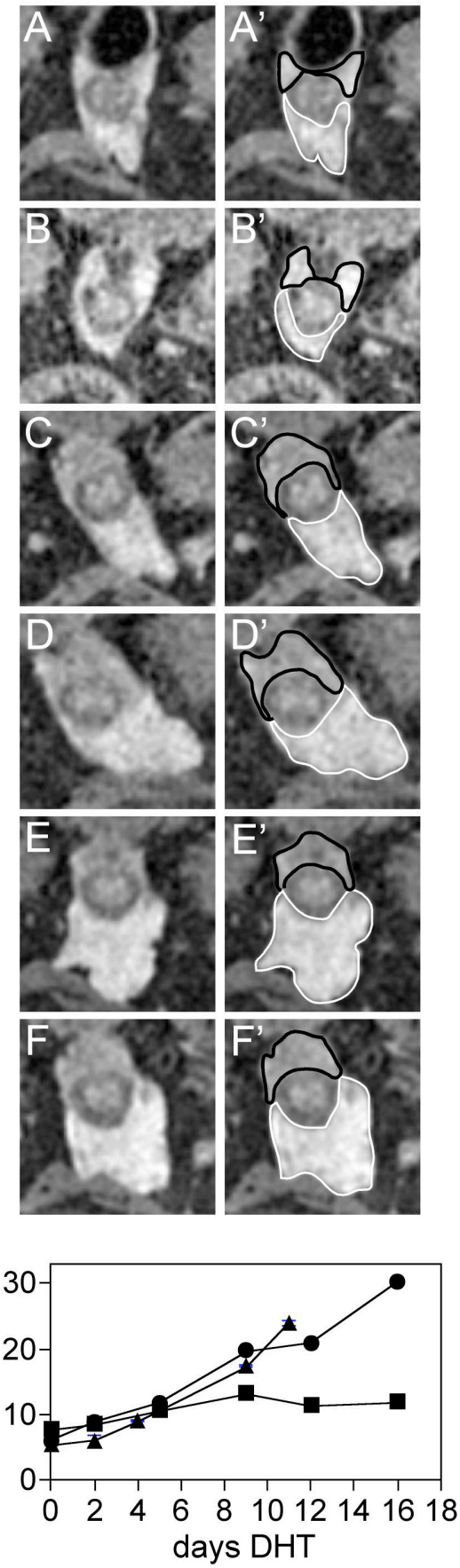
A
A'
B
B'
C
C'
D
D'
E
E'
F
F'
G
volume (mm3)
30
20
10
0
0 2 4 6 8 10 12 14 16 18
days DHT

FOXO3a mediates the androgen-dependent regulation of FLIP and contributes to TRAIL-induced apoptosis of LNCaP cells

Andrew N. Cornforth[1], Kent L. Nastiuk[1], Elham Khanifar[1] and John J. Krolewski*[,1,2]

[1]Department of Pathology and Laboratory Medicine
[2]Chao Family Comprehensive Cancer Center
School of Medicine
University of California, IRVINE
Irvine, CA 92697, USA

*Correspondence: JJ Krolewski, Department of Pathology and Laboratory Medicine, School of Medicine, University of California, IRVINE, Medical Sciences I D450, Irvine, CA 92697-4800; E-mail: jkrolews@uci.edu ; Phone: 949-824-4089

Running title: Androgens and FOXO3a regulate FLIP

Keywords: FLIP, androgen, Forkhead, TRAIL, prostate cancer, apoptosis

Abstract

Androgen withdrawal-induced apoptosis is deregulated in androgen refractory prostate cancer. Androgens have been shown to positively regulate expression of the anti-apoptotic FLICE-like inhibitory protein (FLIP) and reduced FLIP expression precedes apoptosis after androgen withdrawal. In this report, we show that FLIP protein expression is down-regulated in castrated rats while in LNCaP cells, androgens regulate FLIP in a manner that is dependent on phosphoinositol-3-kinase (PI3K) and Akt signaling. Specifically, treatment of LNCaP cells with LY294002, or expression of either PTEN or a non-phosphorylatable form of FOXO3a (FOXO3aTM), down-regulates FLIP protein and mRNA. Conversely, treatment with androgens in the absence of PI3/Akt signaling, or following expression of FOXO3aTM, leads to increased FLIP expression. A FOXO3a binding site was identified in the FLIP promoter and found to be necessary for the combined effects of androgens and FOXO3a on the FLIP promoter. Finally, LNCaP cells are sensitized to TRAIL apoptosis by restoration of PTEN expression, or by treatment with LY294002, and are subsequently rescued by treatment with androgens. Expression of FOXO3aTM produces a similar, but less pronounced, effect on TRAIL apoptosis that can also be rescued by treatment with androgens, suggesting that FOXO3a plays a role in androgen withdrawal induced apoptosis. [197 words]

Introduction

Prostate cancer is the third leading cause of cancer death in men in the US (Jemal et al., 2006). Most deaths are due to the resistance of advanced stage cancers to androgen deprivation therapy (Daskivich & Oh, 2006) which is currently the only effective therapy for metastatic disease. Androgen withdrawal induced apoptosis (AWIA) is a well defined physiological event responsible for homeostasis of the prostate. It is likely that the molecular mechanisms governing AWIA are deregulated in androgen-independent prostate cancer (Kyprianou & Isaacs, 1988). Thus, investigating AWIA may identify novel targets for therapy.

Signaling pathways mediated by phosphoinositol-3-kinase (PI3K), Akt and PTEN control multiple biological processes including proliferation and apoptosis. Alterations in the corresponding genes have

been linked to the pathogenesis of prostate cancer in mice and humans (Majumder & Sellers, 2005). In particular, tissue-specific deletion of PTEN induces prostate cancer in murine models and either loss of PTEN expression, or inactivating mutation, is detected in most late stage human cancers. Moreover, PTEN loss correlates with progression to androgen independence (Bertram et al., 2006). PTEN loss constitutively activates PI3K/Akt signaling and protects cells from apoptotic stimuli while deregulating cell cycle progression. Akt mediates its effects via a host of cell cycle and apoptotic regulating proteins (Cully et al., 2006). For example, Forkhead transcription factor class-O family (FOXO) members are sequestered in the cytoplasm following phosphorylation by Akt (Brunet et al., 1999). In the absence of Akt kinase activity FOXO proteins localize to the nucleus and stimulate gene transcription. Androgens negatively regulate the pro-apoptotic effects of constitutively active (non-phosphorylated) FOXO transcription factors (Huang et al., 2004; Li et al., 2003) and FOXO3a activity is reduced in an androgen independent variant of LNCaP cells (Lynch et al., 2005). Importantly, high level Akt activation in PTEN-null LNCaP cells protects against tumor necrosis factor-related apoptosis inducing ligand (TRAIL) mediated apoptosis (Nesterov et al., 2001). In contrast, normal prostate epithelial cells are sensitive to TRAIL apoptosis (Nesterov et al., 2002).

Sensitivity to death receptor mediated apoptosis can be regulated by the FLICE-like inhibitory protein (FLIP), a proteolytically inactive homologue of caspase-8 (Roth & Reed, 2004). FLIP regulation by androgens has been demonstrated in our previous *in vivo* studies (Nastiuk et al., 2003) and *in vitro* by others (Gao et al., 2005). Moreover, FLIP over-expression correlates with progression to androgen independence (Gao et al., 2005). FLIP is regulated by PI3K/Akt signaling (Panka et al., 2001) and in endothelial cells FLIP is negatively regulated by FOXO3a (Skurk et al., 2004). Down-regulation of FLIP sensitizes prostate cancer cells to TRAIL apoptosis (Zhang et al., 2004). Based on these reports, we investigated the hypothesis that FLIP expression, and TRAIL apoptosis, are coordinately regulated by the androgen receptor (AR) and FOXO3a.

Results

Androgens differentially regulate FLIP protein levels in normal and neoplastic prostate

Previously we demonstrated that, following castration, *FLIP* mRNA levels decline in prostate in advance of the involution and apoptosis of the gland, suggesting FLIP contributes to the regulation of AWIA (Nastiuk et al., 2003). To determine if FLIP protein also declines during AWIA, protein was extracted from the prostates of intact rats or from rats castrated 24 h earlier. An MBP-DED fusion protein was employed to recover FLIP from the extracts (see Materials and methods) prior to immunoblotting with anti-FLIP (Figure 1). The 55 kD $FLIP_L$ protein, as well as smaller amounts of the 43 kD caspase-8 cleavage product, was detected in two intact animals but not in three castrated rats. At 24 h post-castration, there is no detectable nucleosomal fragmentation or involution of the rat prostate (Nastiuk et al., 2003), indicating FLIP protein declines prior to the onset of apoptosis.

Next, androgen regulation of FLIP expression was examined in the PTEN-deficient LNCaP prostate cancer cell line. Cells were incubated for 24 h in media containing androgen-depleted charcoal-dextran stripped serum (CDS) and then treated with the synthetic androgen R1881. PSA rose as expected but, unexpectedly, FLIP was down-regulated (Figure 2a) indicating FLIP is regulated in an opposite manner in these transformed human prostate epithelial cells compared to rat prostate

glands. Quantitation of a time course immunoblot (Figure 2b) showed a 50% reduction in FLIP protein 12-24 h after treatment with R1881. Phospho-Akt levels were unaffected by R1881 (Figure 2b, upper band in top panel).

Androgens up-regulate FLIP following inhibition of PI3K

FLIP levels have been shown to decline in many cell lines following inhibition of PI3K/Akt signaling (Panka et al., 2001). When LNCaP cells were treated with the PI3K inhibitor LY294002 (20 μM) after incubation in 10% CDS, FLIP levels decreased (Figure 3a) concurrent with a decline in phospho-Akt. Time course analysis revealed that this decrease begins 2 h after the addition of LY294002 (Figure 3b). Since androgens protect against apoptosis induced by PI3K inhibition (Kimura et al., 2001) and since FLIP can inhibit death receptor ligand induced apoptosis, we tested the effects of androgens on FLIP expression when PI3K/Akt signaling is repressed. LNCaP cells were grown in R1881 and treated with the PI3K inhibitor LY294002 (20 μM) for an additional 24 h. FLIP protein was up-regulated in response to increasing concentrations of R1881 only when PI3K was inhibited (Figure 4a). PSA levels increased in response to R1881 even in the presence of LY294002. A decrease in phospho-Akt was detected in response to R1881 in this experiment, but this effect was not seen in the time course analysis (Figure 2b). The effect of androgen treatment on FLIP protein expression was mirrored at the mRNA level as measured by quantitative PCR (Figure 4b). Specifically, $FLIP_L$ mRNA levels increased in response to androgen treatment when PI3K was inhibited by LY294002.

Androgen induction of FLIP *transcription requires a Forkhead binding site in the* FLIP *promoter*

A TRANSFAC (Matys et al., 2003) search of the FLIP promoter identified a Forkhead consensus binding site (TGTTTAC) at -65 to -58 bp while a previous report (Gao et al., 2005) identified androgen response elements (AREs) within exon 1. As diagrammed in Figure 5a, three reporter constructs were made to investigate the Forkhead binding site. When LNCaP cells were transfected with these reporters, relatively little luciferase activity was detected whether cells received androgens or not (Figure 5b, left half). However, when the reporter spanning –212 to +250 bp was co-transfected with a cDNA encoding constitutively active FOXO3a (FOXO3aTM), luciferase activity was detected in the absence of androgens and a significant induction was observed upon R1881 addition (Figure 5b, right half). FOXO3aTM is mutated at three Akt phosphorylation sites and thus will localize to the nucleus even in the presence of constitutive Akt signaling. Androgen induction of luciferase activity was largely eliminated when reporters lacked the Forkhead element (due either to deletion or mutation of the TGTTTAC motif; Figure 5b). To confirm that FOXO3a regulates the FLIP response to androgens, a dominant-negative form of FOXO3aTM was constructed by deleting the transactivation domain (Skurk et al., 2004). This construct inhibited the inductive effects of full length FOXO3aTM on the FLIP promoter in response to androgens (Figure 5c, middle column). We also found that a DNA binding mutant (FOXO3aTM-H215R) had a significantly reduced inductive effect on the FLIP promoter reporter activity in response to androgens (Figure 5c, right side). Thus, androgens and active FOXO3a synergistically activate FLIP transcription via a newly identified Forkhead binding motif.

Androgens up-regulate FLIP in LNCaP cells expressing FOXO3aTM

The results in Figure 5 suggest that androgen dependent increases in FLIP protein and mRNA observed in Figure 4 might result from increases in gene transcription mediated by FOXO3a acting with the AR. To test this, LNCaP cells were treated with R1881, or left untreated , and then transfected with either vector, or FLAG-tagged FOXO3a or FOXO3aTM cDNAs (Figure 6a). In cells receiving vector, R1881 down-regulated FLIP (lanes 1-2), similar to Figure 2a. Expression of FOXO3aTM in the absence of androgens also down-regulated FLIP (lanes 1 or 3 versus 5), similar to the effects seen with the PI3K inhibitor LY294002 (Figure 3) and similar to previous reports in endothelial cells (Skurk et al., 2004). However, in cells transfected with FOXO3aTM, R1881 treatment significantly increased FLIP expression (lanes 5-6). When FOXO1a was employed in similar experiments, FLIP expression was not androgen regulated (Figure 6b), indicating specificity for the effects of FOXO3a in LNCaP cells. Similar to the effect of LY294002 (Figure 4), R1881 induces FLIP in LNCaP cells complemented with PTEN (Figure 6c). The level of phospho-Akt was reduced in response to PTEN re-expression (data not shown). Quantitative RT-PCR of mRNA from the samples in Figure 6a revealed that the pattern of $FLIP_L$ mRNA expression is similar to that of FLIP protein. Specifically, introduction of FOXO3aTM or PTEN down-regulates *FLIP* mRNA relative to untransfected LNCaP cells with constitutive Akt signaling (Figure 6d, white bars). Moreover, R1881 addition to cells expressing FOXO3aTM or PTEN up-regulates *FLIP* mRNA (Figure 6d, black bars). Thus, FOXO3aTM and PTEN effect androgen regulation of FLIP protein and mRNA expression in a manner comparable to LY294002 (Figure 4).

Androgens rescue TRAIL-induced apoptosis in LNCaP cells expressing PTEN or FOXO3aTM

To determine if the regulation of FLIP by androgens in response to inhibition of PI3K/Akt signaling is physiologically relevant, we investigated TRAIL mediated apoptosis. LNCaP cells were cultured in the presence or absence of R1881 and LY294002, treated with TRAIL and assayed for Annexin V and 7-amino-actinomycin D (7-AAD) staining as indicators of apoptosis. When PI3K signaling was inhibited by LY294002, TRAIL induced cell death (Figure 7, left side). Exposure to R1881 partially rescued these cells from apoptosis (Figure 7, right side), consistent with our findings that androgens increased the level of the anti-apoptotic FLIP protein under these same conditions (Figure 4).

Since expression of either PTEN or FOXO3aTM in LNCaP cells mimics the effects of LY294002 on FLIP expression, we hypothesized that transfection of these cDNAs should also sensitize cells to TRAIL apoptosis. Androgen treatment in the presence of reduced Akt signaling, by increasing FLIP, should then rescue transfected cells from apoptosis. Indeed, restoring PTEN expression by transfection lead to significant apoptosis even in the absence of TRAIL (Figure 8b, far left). Apoptosis was further enhanced by TRAIL, but prevented when R1881 was added prior to TRAIL treatment (Figure 8b, diagonally-stripped bars). This is visualized in representative plots from the FACS analysis (Figure 8a). In PTEN transfected cells there is a significant shift of the cell population from the lower left quadrant (live cells, not staining with either Annexin V or 7-AAD) to the lower right quadrant (apoptotic cells staining with Annexin V) following the addition of TRAIL. R1881 prevents this shift. FOXO3aTM also induced TRAIL sensitivity, which could be partially rescued by treatment with R1881 (Figure 8b, stippled bars). FACS plots in Figure 8a

demonstrate the appearance of apoptotic cells in the lower right quadrant of TRAIL treated cells and a corresponding reduction when R1881 is added.

Discussion

Androgens are necessary for the maintenance of the prostate, as demonstrated by AWIA of luminal secretory epithelium following castration (Kyprianou & Isaacs, 1988). TGFß plays a key role (Martikainen et al., 1990) and caspase-3 activation has been implicated (Marti et al., 1999), but the role of death receptors such as Fas remains uncertain (de la Taille et al., 1999; Sugihara et al., 2001; Suzuki et al., 1996). Our previous studies demonstrated that mRNA levels of FLIP, a catalytically inactive analogue of caspase-8 which negatively regulates death receptors, declined prior to the onset of castration induced apoptosis (Nastiuk et al., 2003). This suggests that FLIP is an androgen regulated protein involved in the control of AWIA. Subsequently, LNCaP cells expressing FLIP were reported to form androgen-independent tumors at a higher rate than parental cells (Gao et al., 2005). LNCaP derived tumors over-expressing the caspase-8 inhibitor crmA behaved similarly (Srikanth & Kraft, 1998). Also, FLIP levels were elevated in androgen-independent human cancers (Gao et al., 2006), supporting the hypothesis that FLIP inhibits caspase-8 to regulate AWIA in normal and neoplastic prostate.

In the first part of this report we demonstrate that FLIP is regulated by androgens *in vitro* in a manner resembling its regulation *in vivo*, and we characterize the molecular mechanisms regulating FLIP expression in prostate epithelium. Figure 1 confirmed that, as we observed for *FLIP* mRNA (Nastiuk et al., 2003), FLIP protein declined in normal rat prostate 24 h after castration, before the appearance of any significant involution or biochemical evidence of apoptosis is expected (see Nastiuk et al., 2003). Immunohistochemical staining of prostate glands from castrated mice demonstrated a temporally similar pattern of FLIP expression (Gao et al., 2006). The timing of FLIP protein modulation suggests that down-regulation either facilitates the apoptotic effects of a pre-existing death ligand or occurs coordinately with the up-regulation of a death ligand(s).

To further characterize androgen regulation of FLIP expression, we employed the human prostate cancer derived cell line LNCaP as an *in vitro* model. LNCaP has a deletion of one PTEN allele (Hermans et al., 2004) and a frameshift mutation in the other (Li et al., 1997), producing constitutive PI3K/Akt signaling, which likely drives survival and proliferation. FLIP inhibits death receptor driven apoptosis and therefore also promotes cell survival. Moreover, constitutive PI3K/Akt signaling increases FLIP in many cell lines, including the androgen independent prostate cancer lines PC3 and DU145 (Panka et al., 2001). Our data demonstrate that in androgen responsive LNCaPs, treatment with the PI3K inhibitor LY294002 decreases FLIP protein (Figure 3) and mRNA (Figure 4b). Similarly, re-introduction of PTEN decreased FLIP protein (Figure 6a, lane 1 versus Figure 6c, lane1) and mRNA (Figure 6d). When we examined the effects of androgens on FLIP expression, in the constitutive Akt signaling state seen in LNCaP cells (Figure 2), FLIP was down-regulated, the opposite of the response in normal rat prostate. However, when PI3K was inhibited with LY294002 (Figure 4) or Akt signaling was inhibited with PTEN (Figure 6), androgens up-regulated FLIP expression, as observed in the normal rat prostate. Levels of phospho-Akt are low or undetectable in most samples of benign human prostate epithelium (Ayala et al., 2004; Liao et al., 2003). Thus, when Akt signaling activity in LNCaP is reduced to resemble the level observed in normal epithelium, FLIP is positively regulated by

androgens, consistent with a possible role in AWIA. Gao et al., (2005) also demonstrated androgens up-regulate FLIP in LNCaP, but in contrast to our data, the effects apparently did not require inhibition of PI3K/Akt signaling. These authors demonstrated androgen dependent up-regulation of *FLIP* mRNA, but did not examine FLIP protein regulation. They also identified the androgen-responsive elements within exon I (Figure 5a), although this data mainly derived from reporter gene studies in PC3 cells.

Our identification of a Forkhead box element within the FLIP upstream regulatory region (Figure 5a) suggested that a FOXO transcription factor might mediate Akt signaling effects. Indeed, Figures 5 and 6 indicate FOXO3a is a primary mediator of PI3K signaling on FLIP expression, and demonstrate a strong effect at the transcriptional level via FOXO3a binding to the FLIP promoter. Our results are in agreement with a report that FOXO3a down-regulates FLIP in endothelial cells (Skurk et al., 2004). Deciphering the mechanism of AR and FOXO3a cooperation in regulating FLIP will require additional experimentation. A direct interaction between these two transcription factors is a likely possibility as other Forkhead family members (FOXA1and FOXO1a) bind AR (Gao et al., 2003; Li et al., 2001). Notably, in the case of the FOXA1 regulated PSA and Probasin genes, Forkhead elements are located near AREs, similar to the structure of the FLIP promoter.

Previously, androgens have been shown to inhibit PTEN or FOXO1a induced apoptosis of prostate cancer cells (Huang et al., 2004; Li et al., 2003; Li et al., 2001), while PTEN expression was shown to sensitize LNCaPs to TRAIL (Yuan & Whang, 2002). Consistent with FLIP regulation of death receptor mediated apoptosis and our observations on FLIP expression described above, we observed that LY294002 treatment (Figure 7), or PTEN/FOXO3aTM expression (Figure 8) sensitized LNCaP cells to TRAIL apoptosis and, furthermore, that androgen treatment rescued this effect. Androgens may play a protective role by synergistically up-regulating FLIP expression in a manner that is dependent on active FOXO3a. However, while our immunoblotting data indicate that FOXO3a accounts for most of the PTEN effect on FLIP expression in response to androgens (compare Figure 6a, lanes 5-6 and Figure 6c), the FACS data in Figure 8 indicate that FOXO3aTM only accounts for a portion of the PTEN sensitizing effect on TRAIL mediated apoptosis. It is likely that other pro-apoptotic, PTEN-driven events account for the remainder of the effect (Majumder & Sellers, 2005). Finally, our findings that PI3K/Akt signaling, via FOXO3a, modulates androgen regulation of FLIP might provide insight into the process of prostate carcinogenesis. Specifically, androgen deprivation may be ineffective in down-regulating FLIP in prostate tumor cell subpopulations lacking PTEN, thereby favoring the survival or growth of these cells. This may help account for the predominant PTEN-negative status of androgen independent tumors.

Materials and methods

Cell lines and reagents

HEK293T cells (H. Young, Columbia University, College of Physicians and Surgeons) were grown in DMEM plus 10% fetal bovine serum (FBS). LNCaP cells (LNCaP-FCG; ATCC) were maintained in RPMI-1640 plus 10% FBS, 1 mM sodium pyruvate and 1 mM HEPES, pH 7.4. LNCaP cells were passaged no more than 24 times. CDS was prepared by treating FBS with 0.5% activated charcoal (Norit A, Sigma) and 0.05% dextran T-70 (Pharmacia) while heating at 55°C for 30 min. Prior to treatment with androgens, LNCaP cells were washed twice with PBS and incubated in phenol red-free RPMI containing 10% CDS for 24 h. The synthetic androgen methyltrienolone (R1881; Dupont) was dissolved in ethanol. LY294002 (Cayman) was dissolved in

dimethylsulfoxide (DMSO). Soluble recombinant human TRAIL (Biomol), corresponding to residues 114-281, was diluted in 20 mM Tris-HCl, 300 mM NaCl, 0.006% Tween-20, 1% sucrose, 0.05 mM DTT.

Plasmid constructs

The -212 to +250 bp FLIP promoter was PCR amplified from BAC clone RP11-536I18 (CHORI) and inserted into the KpnI and XhoI sites of pGL3 Basic (Promega). A deletion construct of this promoter fragment was made using the MluI site at -52. Overlap PCR was used to mutate the Forkhead transcription factor binding site at -65 to -58 from TGTTTAC to TGgaaAC. An amino-terminal FLAG-tagged FOXO3a constructs were made by subcloning a cDNA encoding the triple FOXO3a mutant (T32A/S253A/S315A; M. Greenberg, Harvard Medical School), into pFLAG-CMV2 (Sigma). A dominant negative FOXO3aTM construct was made by deleting the transactivation domain as previously reported (Skurk et al., 2004) and a plasmid encoding FLAG-FOXO3aTM H215R was prepared by restriction fragment cloning from pECE-FOXO3aTM-H215R (D. Fruman, University of CA, Irvine) into pFLAG-CMV2. The plasmid pMT2T-PTEN-HA, encoding a carboxyl-terminal tagged protein, was made by PCR cloning full-length human PTEN into pMT2T-HA. FOXO1a constructs (Tang et al., 1999) were from K. Guan (University of Michigan, Ann Arbor). A plasmid encoding a fusion between maltose binding protein (MBP) and the rat caspase-8 DEDs (residues 1-181) was prepared by Pfu PCR amplification of the caspase-8 region and cloning into the pMAL-2c vector (New England Biolabs). All PCR generated constructs were sequenced.

Immunoblotting

LNCaP cells were harvested by pipetting and lysed on ice for 10 min in NP40 lysis buffer (1% NP40, 1 mM $NaVO_4$, 100 mM NaF, 2.5 µM $ZnCl_2$, 10% glycerol, 0.2 mM phenylmethylsulphonylfluoride and protease inhibitor cocktail (Sigma) in Tris-buffered saline solution (TBS)). The protein concentration of cleared lysates was determined by BCA assay (Pierce) and 40-50 µg of total protein was electrophoresed and transferred to nitrocellulose.

Mature Sprague-Dawley rats (~350 g) were castrated under methoxyflurane anesthesia and 24 h later animals were sacrificed and the ventral lobe of the prostate was rapidly removed and snap frozen. Tissue was pulverized and protein extracted from individual prostates using 10 volumes of the lysis buffer described above, plus zVAD-Fmk (5 mM; Biomol). Because we were unable to immunoprecipitate FLIP efficiently, we employed the homotypic affinity of DED domains to recover FLIP from rat tissues. Briefly, lysates were sonicated and 750 mg of protein from a $1.5x10^4$ *g* supernatant were pre-cleared with 300 mg of amylose beads. MBP-rat caspase-8 DED fusion protein was coupled to amylose beads with glutaraldehyde. The cleared lysate was incubated for 4 h with 30 mg of coupled MBP-DED protein, and bound protein was immunoblotted. To confirm equal amounts of protein in each of affinity precipitation, 50 µg of cleared lysate protein were immunoblotted in parallel with anti-actin.

Immunoblots were sequentially reacted with primary antibody, peroxidase-conjugated secondary antibody and SuperSignal West Pico chemiluminescense substrate (Pierce). Blots were exposed to film or a cooled charged-coupled digital camera (Kodak 4000R). Primary antibodies were directed against human $FLIP_{L/S}$ (1:250, NF6, Alexis), PSA (1:500, Dako), FLAG (1:1000, M2, Sigma), phospho-Akt-S473 and Akt (both 1:500, Cell Signalling), human PTEN (1:500, 6H2.1, Cascade BioScience), human actin (AC-15, Sigma) and rat FLIP (a rabbit polyclonal antibody raised against the peptide QVEESLDEDEKEC, corresponding to residues 13-24).

Quantitative RT-PCR

RNA (100 ng), extracted with TRIzol reagent (Invitrogen), was reverse transcribed using SuperScript II MMLV reverse transcriptase (Invitrogen) and real-time PCR was performed with SYBER Green (Molecular Probes) as described (Nastiuk et al., 2003). The primer pairs, which spanned at least one intron, are: for $FLIP_L$, 5'-AGGAGCAGGGACAAGTTACAGG-3' and 5'-CTAGGGGCTTGCTCTTCATCTT-3'; and for ß-actin, 5'-CAGAGCAAGAGAGGCATC-3' and 5'-CAGAGGCATACAGGGACAG-3'. The mRNA copy numbers were determined by comparing the amplification profiles (log fluorescence vs. cycle number) of the SYBER Green signal recorded 2°C below the duplex melting point with serially diluted internal

standards of the same target gene. $FLIP_L$ copy numbers were normalized using ß-actin copy numbers. Each reverse transcription reaction was performed in triplicate and real-time PCR reactions were carried out in triplicate for each sample. Statistical analysis was performed by paired Student's t-test.

Transfection

LNCaP cells ($1x10^5$) were seeded on 24 well plates two days prior to lipofection (LipofectAMINE, Invitrogen) in antibiotic-free RPMI with 10% CDS. Briefly, 100 ng of firefly-luciferase reporter construct plus 25 ng of FOXO3a expression construct and 25 ng of constitutive Renilla luciferase reporter were transfected in serum free RPMI (without phenol red). DNA content was adjusted by the addition of vector. After 3 h, LNCaP cells were incubated in 1 nM R1881 or vehicle in 10% CDS/RPMI for 24 h. LNCaP cells ($2x10^6$ cells) were nucleofected at the T09 setting in buffer R (Nucleofector II, Amaxa).

Reporter gene assays

Cells were harvested, lysed and assayed simultaneously for firefly and Renilla luciferase activity using commercial reagents (Promega). Relative light units (RLU) were calculated by dividing firefly activity by the corresponding Renilla activity value.

FACS analysis of apoptosis

LNCaP ($3-5x10^5$) cells were detached from dishes by pipetting and then resuspended in PBS plus 0.25% trypsin for 5 min to disrupt clumped cells. Trypsin was inactivated by the addition of 10% CDS, the cells were washed in Hank's balance salt solution (HBSS), and incubated in 0.1 mL HBSS plus R-phycoerythrin conjugated Annexin-V (1:100, Invitrogen) and 7-aminoactinomycin D (1:200, Invitrogen) for 15 min at room temperature in the dark. Cells were washed, resuspended in HBSS and analyzed by two-color FACS (BD Biosciences). Data was analyzed using FloJo software (Tree Star). Statistical analysis was performed by paired Student's t-test.

Acknowledgements

This research was supported by grant PC030937 from the US Army Prostate Cancer Research Program. A.N.C. was supported by an PHS training grant (5T32CA009054).

References:

Ayala, G., Thompson, T., Yang, G., Frolov, A., Li, R., Scardino, P., Ohori, M., Wheeler, T. & Harper, W. (2004). *Clin Cancer Res*, **10,** 6572-8.

Bertram, J., Peacock, J.W., Fazli, L., Mui, A.L., Chung, S.W., Cox, M.E., Monia, B., Gleave, M.E. & Ong, C.J. (2006). *Prostate*, **66,** 895-902.

Brunet, A., Bonni, A., Zigmond, M.J., Lin, M.Z., Juo, P., Hu, L.S., Anderson, M.J., Arden, K.C., Blenis, J. & Greenberg, M.E. (1999). *Cell*, **96,** 857-68.

Cully, M., You, H., Levine, A.J. & Mak, T.W. (2006). *Nat Rev Cancer*, **6,** 184-92.

Daskivich, T.J. & Oh, W.K. (2006). *Curr Opin Urol*, **16,** 173-8.

de la Taille, A., Chen, M.W., Shabsigh, A., Bagiella, E., Kiss, A. & Buttyan, R. (1999). *Prostate*, **40,** 89-96.

Gao, N., Zhang, J., Rao, M.A., Case, T.C., Mirosevich, J., Wang, Y., Jin, R., Gupta, A., Rennie, P.S. & Matusik, R.J. (2003). *Mol Endocrinol*, **17,** 1484-507.

Gao, S., Lee, P., Wang, H., Gerald, W., Adler, M., Zhang, L., Wang, Y.F. & Wang, Z. (2005). *Mol Endocrinol*, **19,** 1792-1802.

Gao, S., Wang, H., Lee, P., Melamed, J., Li, C.X., Zhang, F., Wu, H., Zhou, L. & Wang, Z. (2006). *J Mol Endocrinol*, **36,** 463-83.

Hermans, K.G., van Alewijk, D.C., Veltman, J.A., van Weerden, W., van Kessel, A.G. & Trapman, J. (2004). *Genes Chromosomes Cancer*, **39,** 171-84.

Huang, H., Muddiman, D.C. & Tindall, D.J. (2004). *J Biol Chem*, **279,** 13866-77.

Jemal, A., Siegel, R., Ward, E., Murray, T., Xu, J., Smigal, C. & Thun, M.J. (2006). *CA Cancer J Clin*, **56,** 106-30.

Kimura, K., Markowski, M., Bowen, C. & Gelmann, E.P. (2001). *Cancer Res*, **61,** 5611-8.

Kyprianou, N. & Isaacs, J.T. (1988). *Endocrinology*, **122,** 552-62.
Li, J., Yen, C., Liaw, D., Podsypanina, K., Bose, S., Wang, S.I., Puc, J., Miliaresis, C., Rodgers, L., McCombie, R., Bigner, S.H., Giovanella, B.C., Ittmann, M., Tycko, B., Hibshoosh, H., Wigler, M.H. & Parsons, R. (1997). *Science*, **275,** 1943-7.
Li, P., Lee, H., Guo, S., Unterman, T.G., Jenster, G. & Bai, W. (2003). *Mol Cell Biol*, **23,** 104-18.
Li, P., Nicosia, S.V. & Bai, W. (2001). *J Biol Chem*, **276,** 20444-50.
Liao, Y., Grobholz, R., Abel, U., Trojan, L., Michel, M.S., Angel, P. & Mayer, D. (2003). *Int J Cancer*, **107,** 676-80.
Lynch, R.L., Konicek, B.W., McNulty, A.M., Hanna, K.R., Lewis, J.E., Neubauer, B.L. & Graff, J.R. (2005). *Mol Cancer Res*, **3,** 163-9.
Majumder, P.K. & Sellers, W.R. (2005). *Oncogene*, **24,** 7465-74.
Marti, A., Jaggi, R., Vallan, C., Ritter, P.M., Baltzer, A., Srinivasan, A., Dharmarajan, A.M. & Friis, R.R. (1999). *Cell Death Differ*, **6,** 1190-200.
Martikainen, P., Kyprianou, N. & Isaacs, J.T. (1990). *Endocrinology*, **127,** 2963-8.
Matys, V., Fricke, E., Geffers, R., Gossling, E., Haubrock, M., Hehl, R., Hornischer, K., Karas, D., Kel, A.E., Kel-Margoulis, O.V., Kloos, D.U., Land, S., Lewicki-Potapov, B., Michael, H., Munch, R., Reuter, I., Rotert, S., Saxel, H., Scheer, M., Thiele, S. & Wingender, E. (2003). *Nucleic Acids Res*, **31,** 374-8.
Nastiuk, K.L., Kim, J.W., Mann, M. & Krolewski, J.J. (2003). *J Cell Physiol*, **196,** 386-93.
Nesterov, A., Ivashchenko, Y. & Kraft, A.S. (2002). *Oncogene*, **21,** 1135-40.
Nesterov, A., Lu, X., Johnson, M., Miller, G.J., Ivashchenko, Y. & Kraft, A.S. (2001). *J Biol Chem*, **276,** 10767-74.
Panka, D.J., Mano, T., Suhara, T., Walsh, K. & Mier, J.W. (2001). *J Biol Chem*, **276,** 6893-6.
Roth, W. & Reed, J.C. (2004). *Vitam Horm*, **67,** 189-206.
Skurk, C., Maatz, H., Kim, H.S., Yang, J., Abid, M.R., Aird, W.C. & Walsh, K. (2004). *J Biol Chem*, **279,** 1513-25.
Srikanth, S. & Kraft, A.S. (1998). *Cancer Res*, **58,** 834-9.
Sugihara, A., Yamada, N., Tsujimura, T., Iwasaki, T., Yamashita, K., Takagi, Y., Tsuji, M. & Terada, N. (2001). *In Vivo*, **15,** 385-90.
Suzuki, A., Matsuzawa, A. & Iguchi, T. (1996). *Oncogene*, **13,** 31-7.
Tang, E.D., Nunez, G., Barr, F.G. & Guan, K.L. (1999). *J Biol Chem*, **274,** 16741-6.
Yuan, X.J. & Whang, Y.E. (2002). *Oncogene*, **21,** 319-27.
Zhang, X., Jin, T.G., Yang, H., DeWolf, W.C., Khosravi-Far, R. & Olumi, A.F. (2004). *Cancer Res*, **64,** 7086-91.

Figure legends

Figure 1 $FLIP_L$ protein is down-regulated in rat prostate following castration. Prostates were harvested from two untreated adult male rats (normal; lanes 2-3) or from three rats 24 h after castration (castrate; lanes 4-6). Tissue was homogenized, FLIP protein affinity precipitated using MBP-linked DED fusion proteins, and the resulting complexes were immunoblotted and probed with anti-FLIP antibody (G878) (see Materials and methods). Lane 1 is from HEK293T cells over-expressing rat $FLIP_L$. About 3% of each tissue homogenate used in the affinity precipitation was immunoblotted with anti-ß-actin.

Figure 2 $FLIP_L$ protein expression is down-regulated in LNCaP cells in response to androgen treatment. (**a**) R1881 dose dependence. LNCaP cells ($1x10^6$) were seeded in media containing 10% FCS. After 24 h, the media was changed to 10% CDS for 24 h followed by the addition of R1881, as indicated. After an additional 24 h, cells were harvested and lysates immunoblotted with indicated antibodies. Ethanol (0.1%) was used as the vehicle control in lane 1. (**b**) Time dependence. Similar to (**a**) except that cells were harvested at the indicated times after the addition of 1 nM R1881 and the upper panel was probed simultaneously with anti-P-Akt and anti-FLIP antibodies (the upper band corresponds to Akt). FLIP levels were quantitated (see Materials and methods), normalized to the ß-actin and then relative to lane 1,

and given below the respective lane numbers. Results in (**a**) and (**b**) are representative of at least three independent experiments.

Figure 3 Inhibition of the PI3 kinase pathway by LY294002 down-regulates $FLIP_L$ protein expression in LNCaP cells. (**a**) LY294002 dose dependence. LNCaP cells were treated and the resulting lysates immunoblotted as in Figure 2a, except that LY294002 was added at the indicated concentrations. DMSO (0.1%) was used a vehicle control in lane 1. (**b**) LY294002 time dependence. Similar to (**a**) except that cells were harvested at the indicated times after the addition of 20 μM LY294002. Chemiluminescence was quantitated as in Figure 2b. Results in (**a**) and (**b**) are representative of at least three independent experiments.

Figure 4 $FLIP_L$ mRNA and protein are both up-regulated by androgens in a manner dependent on the inhibition of the PI3 kinase pathway. **(a)** FLIP protein regulation. LNCaP cells were treated and the resulting lysates immunoblotted as in Figure 2a, except that cells were also incubated in the presence or absence of 20 μM LY294002 for an additional 24 h along with the indicated concentrations of R1881. Vehicle controls were as in Figures 2 and 3. Results are representative of three independent experiments. (**b**) FLIP mRNA regulation. RNA was extracted from LNCaP cells treated as in (**a**) and reverse-transcribed cDNA was used to determine the $FLIP_L$ mRNA copy number by quantitative PCR (see Materials and methods). $FLIP_L$ levels were normalized to the vehicle control sample in the column at the far left to obtain the fold-change in mRNA levels for each treatment condition. RNA from four independent experiments was reverse transcribed and PCR was performed on cDNA prepared in triplicate for each experiment. The p-values for 0 nM versus 10 nM R1881 were <0.01 (single asterisk; for culture receiving DMSO) and <0.05 (double asterisk; for cultures receiving LY2945002).

Figure 5 The -212 to +250 portion of the $FLIP_L$ promoter is synergistically transactivated by FOXO3a and AR. (**a**) Schematic of reporter gene constructs. A region spanning -212 to +250 bp of the $FLIP_L$ promoter was PCR cloned upstream of the pGL3 Basic firefly luciferase reporter gene (see Materials and methods). A Forkhead transcription factor binding site identified by TRANSFAC sequence analysis (boxed F) and previously identified androgen response elements (boxed AREs) are indicated. A truncation mutant (-52 to +250) that lacks the Forkhead binding element was made by restriction digestion at an endogenous MluI site. A mutation of the Forkhead transcription factor binding site was made by site directed mutagenesis (see Materials and Methods). Corresponding boxes on the left indicate shading of the columns in (**b**) and (**c**). The numbering of the FLIP promoter is based on the transcriptional start site specified by Genbank accession number U97074. (**b**) Synergistic effects of FOXO3a and AR require an intact Forkhead binding element. LNCaP cells were transfected (lipofection) with plasmids encoding the luciferase reporters (100 ng) described in (**a**), FOXO3aTM (25 ng) or corresponding pCMV2 vector, and/or treated with 1 nM R1881 as indicated. An SV40 promoter driven Renilla luciferase reporter (25 ng) construct was used to normalize for transfection efficiency. Normalized values are reported as relative luciferase units (RLU). Prior to transfection, cells were incubated in media with 10% CDS with and without R1881. Cells were harvested 18-24 h post-transfection and assayed. (**c**) Synergistic effects of FOXO3a and AR require an intact DNA binding domain in FOXO3a. Similar to (**b**), except that plasmids encoding DN-FOXO3aTM (250 ng) or FOXO3a TMH215R (25 ng) were used as indicated. Data in (**b**) and (**c**) are representative of three independent experiments.

Figure 6 FOXO3aTM or PTEN induced down-regulation of $FLIP_L$ protein and mRNA is inhibited by androgens. (**a**) FOXO3aTM induced down-regulation of $FLIP_L$ protein is inhibited by R1881. LNCaP cells ($2x10^6$) were incubated in media with 10% CDS, with and without R1881 as indicated. Subsequently, these cells were transfected via Nucleofection (see Materials and methods) with 2 μg of vector, FLAG-FOXO3a (WT) or FOXO3aTM (TM) encoding plasmids, further treated with R1881 as indicated, and harvested 10 h later for immunoblotting with the indicated antibodies. (**b**) FOXO1a does not produce the effects of FOXO3a. Similar to (**a**), except FOXO1a constructs were used. (**c**) $FLIP_L$

protein expression in up-regulated by R1881 in LNCaP cells expressing PTEN. Similar to (**a**), except a PTEN construct was used. Data in (**a**), (**b**) and (**c**) are representative of three independent experiments; chemiluminescence was quantitated as in Figure 2b. (**d**) R1881 increases $FLIP_L$ mRNA levels in cells over-expressing FOXO3aTM or PTEN. LNCaP cells were treated and nucleofected as in (**a**), then RNA was extracted, reverse transcribed and PCR amplified as described in Figure 4b. The p-values derived by comparing 0 nM versus 10 nM R1881 were <0.01 (single asterisk; cultures transfected with PTEN) and <0.05 (double asterisk; for cultures transfected with FOXO3aTM). Each data point represents two separate experiments conducted in triplicate.

Figure 7 Androgens partially block apoptosis induced in LNCaP cells by a combination of TRAIL and PI3K inhibition. LNCaP cells were treated as in Figure 4, exposed to 100 ng/mL TRAIL for 18 h, stained with fluorescent-tagged Annexin V and 7-AAD and analyzed by FACS (see Materials and methods). The percentage of live cells (Annexin V and 7-AAD negative cells) is plotted. Each data point represents two separate experiments conducted in triplicate.

Figure 8 Androgens partially block apoptosis induced in LNCaP cells by a combination of TRAIL and PTEN or FOXO3aTM over-expression. (**a**) FACS data. LNCaP cells were pre-treated and nucleofected with the plasmid constructs indicated across the top of the panel, as in Figure 6. Following transfection, cultures were divided into four parts and treated for 18 h with TRAIL (100 ng/mL), and/or R1881 (1 nM), or left untreated in media containing 10% CDS (CDS) as indicated along the left side of the panel. Staining and FACS analysis was as in Figure 7. Representative FACS plots are shown. (**b**) Plot of live cell fraction determined from FACS data. The percentage of live cells (Annexin V and 7-AAD negative cells; lower left quadrants) is plotted for each of the treatment conditions and constructs introduced into the cells. Each data point represents two separate experiments conducted in triplicate. The p-value derived by comparing the indicated pair of columns was <0.05 (double asterisk).

Figure 1

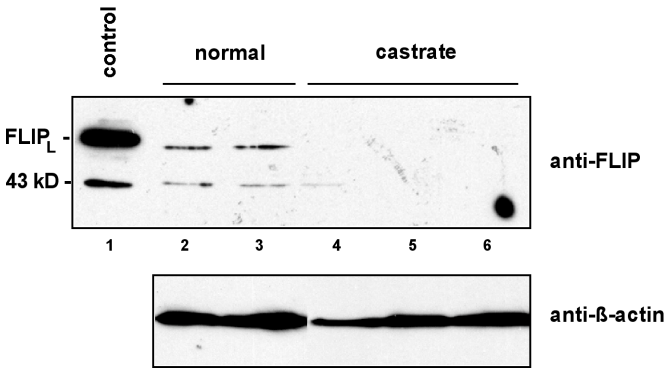
control
normal
castrate
FLIP$_L$ -
43 kD -
anti-FLIP
1
2
3
4
5
6
anti-ß-actin

Figure 2

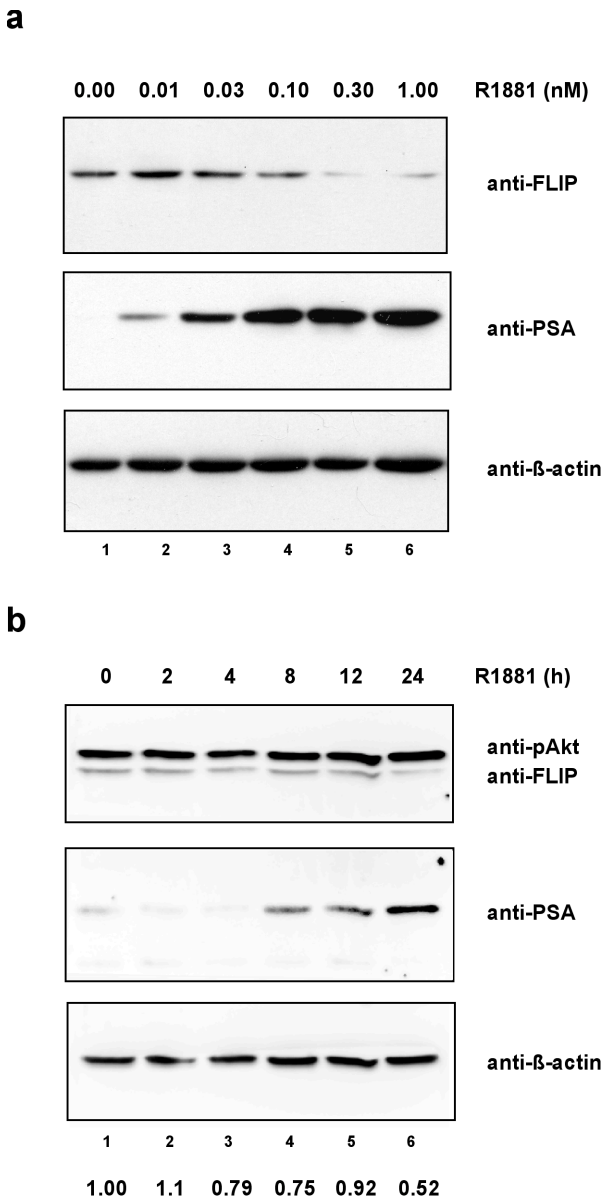
a
0.00 0.01 0.03 0.10 0.30 1.00 R1881 (nM)
anti-FLIP
anti-PSA
anti-ß-actin
1 2 3 4 5 6
b
0 2 4 8 12 24 R1881 (h)
anti-pAkt
anti-FLIP
anti-PSA
anti-ß-actin
1 2 3 4 5 6
1.00 1.1 0.79 0.75 0.92 0.52

Figure 3

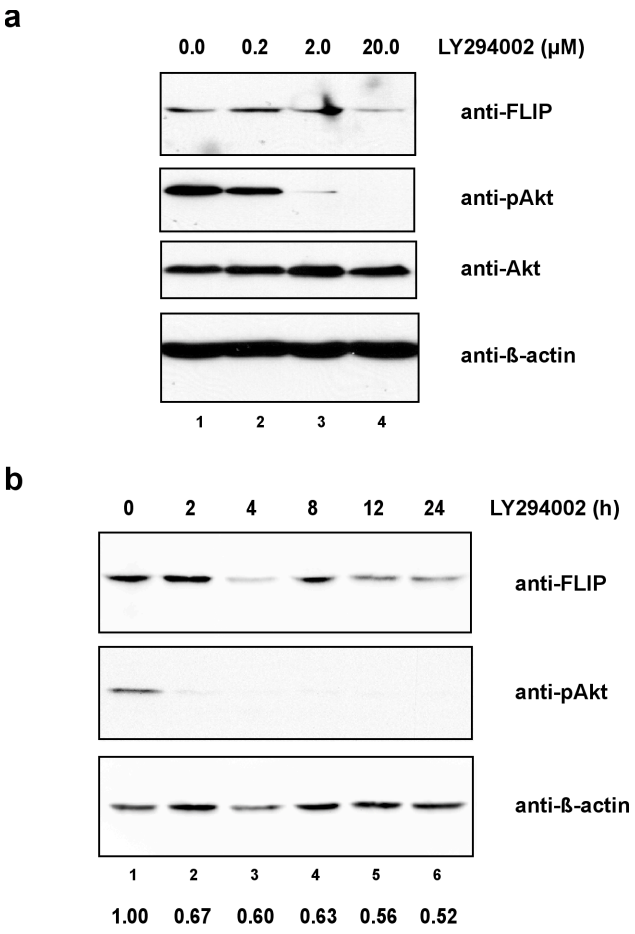
a
0.0
0.2
2.0
20.0
LY294002 (μM)
anti-FLIP
anti-pAkt
anti-Akt
anti-ß-actin
1
2
3
4
b
0
2
4
8
12
24
LY294002 (h)
anti-FLIP
anti-pAkt
anti-ß-actin
1
2
3
4
5
6
1.00
0.67
0.60
0.63
0.56
0.52

Figure 4

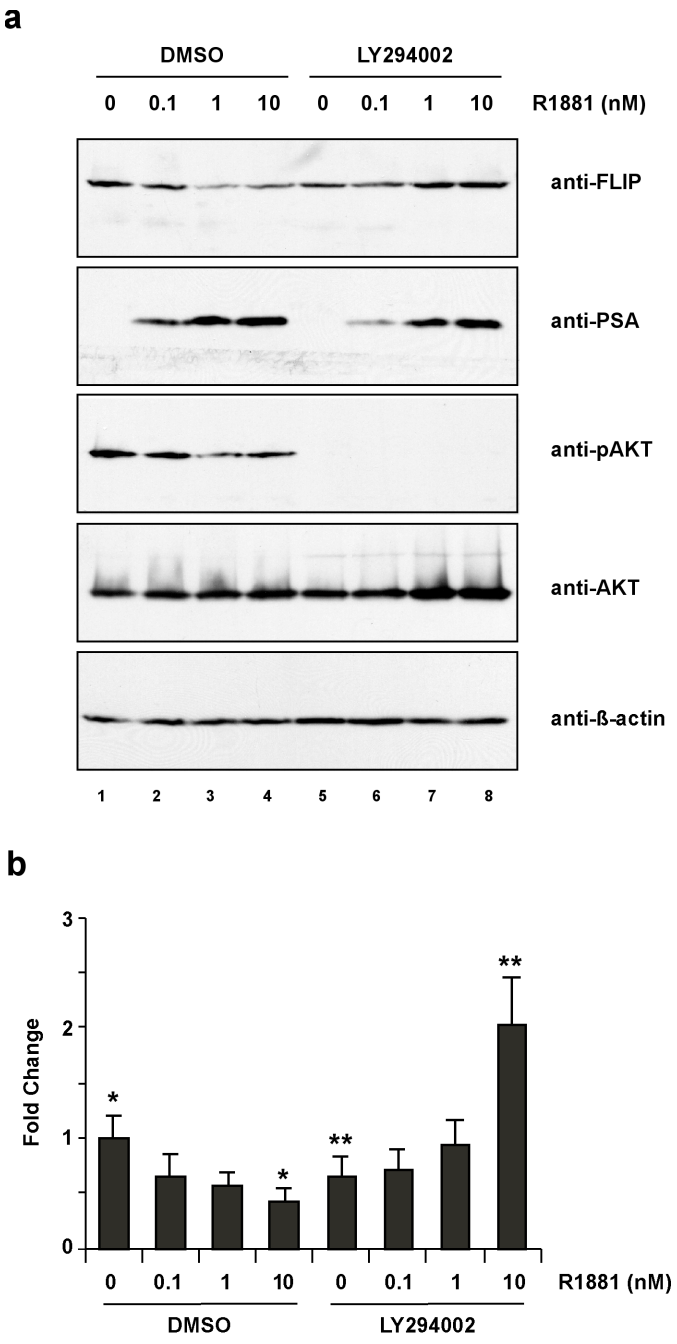
a
DMSO
LY294002
0 0.1 1 10 0 0.1 1 10 R1881 (nM)
anti-FLIP
anti-PSA
anti-pAKT
anti-AKT
anti-ß-actin
1 2 3 4 5 6 7 8
b
Fold Change
3
2
1
0
*
*
**
**
0 0.1 1 10 0 0.1 1 10 R1881 (nM)
DMSO
LY294002

Figure 5

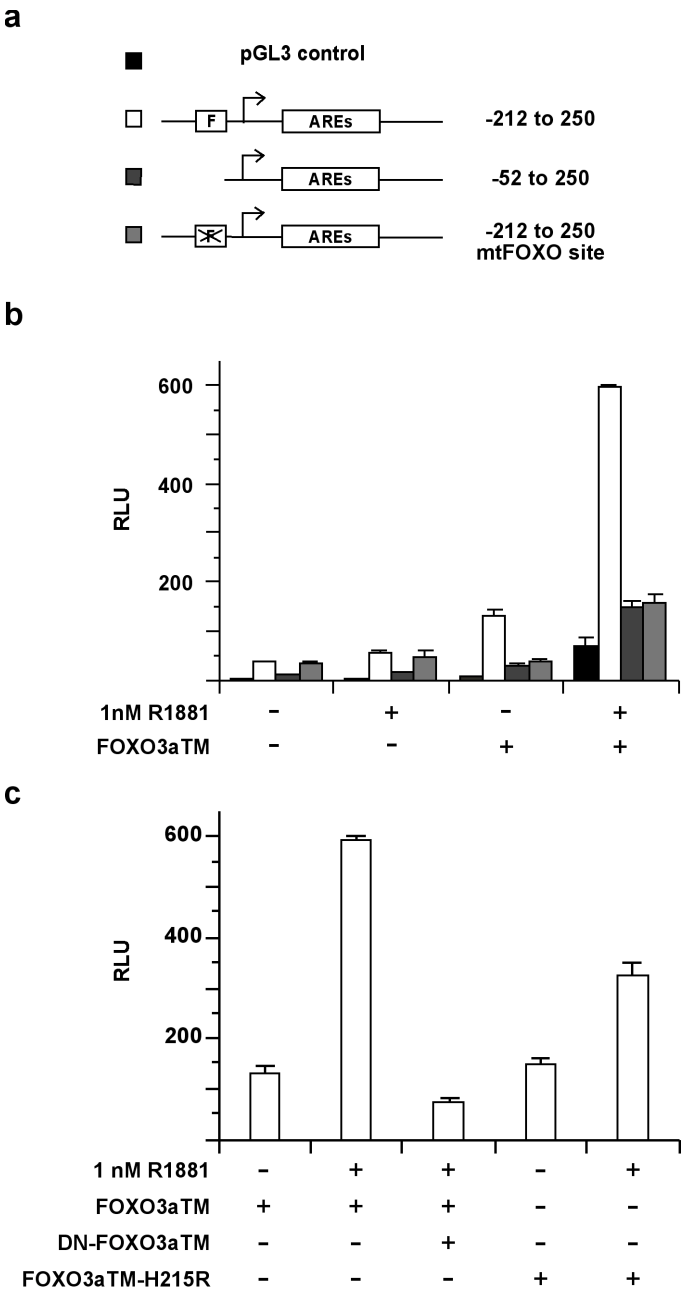
a
pGL3 control
F
AREs
-212 to 250
AREs
-52 to 250
AREs
-212 to 250
mtFOXO site
b
RLU
600
400
200
1nM R1881 - + - +
FOXO3aTM - - + +
c
RLU
600
400
200
1 nM R1881 - + + - +
FOXO3aTM + + + - -
DN-FOXO3aTM - - + - -
FOXO3aTM-H215R - - - + +

Figure 6

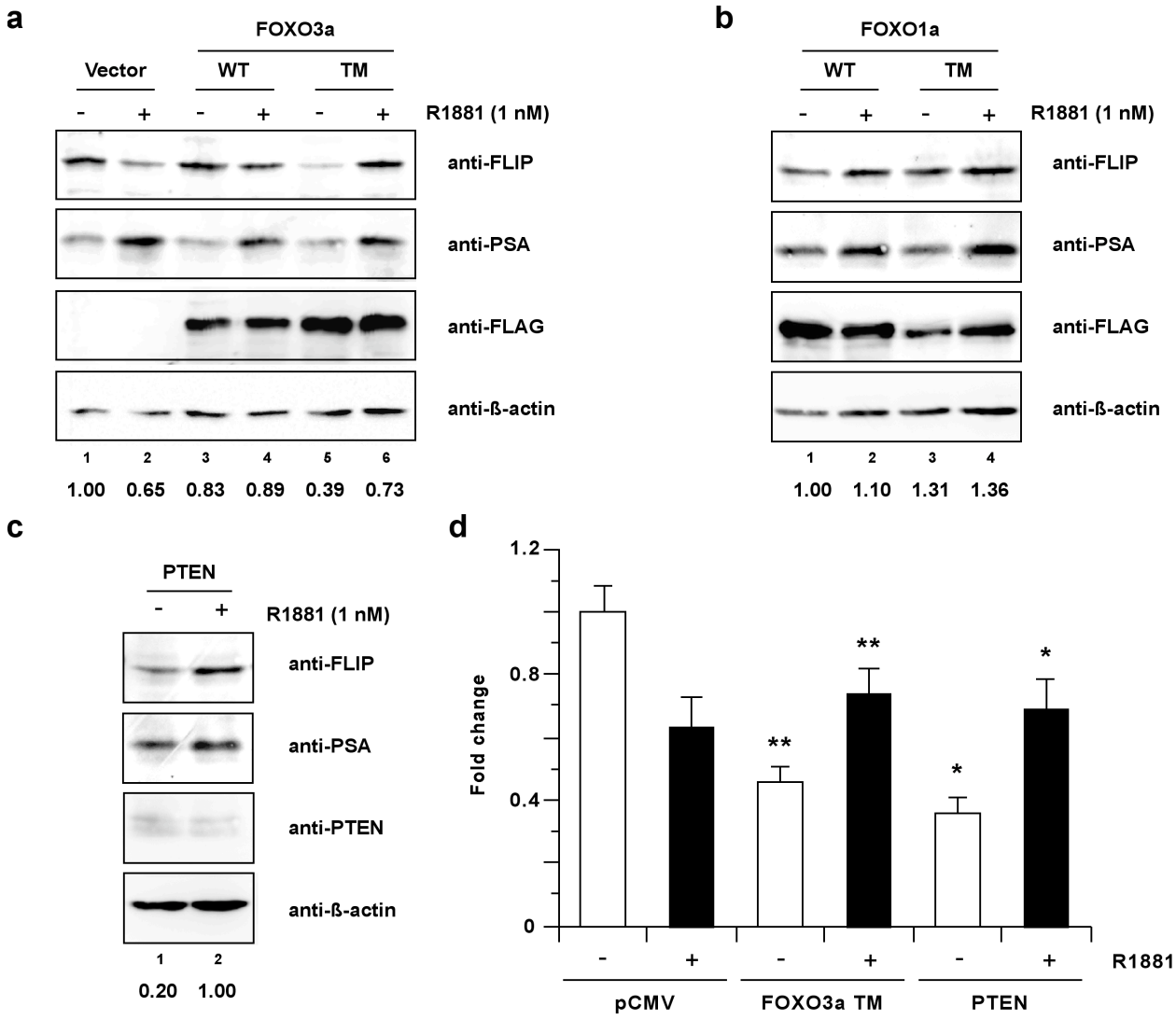
a
FOXO3a
Vector
WT
TM
- + - + - +
R1881 (1 nM)
anti-FLIP
anti-PSA
anti-FLAG
anti-ß-actin
1 2 3 4 5 6
1.00 0.65 0.83 0.89 0.39 0.73
b
FOXO1a
WT
TM
- + - +
R1881 (1 nM)
anti-FLIP
anti-PSA
anti-FLAG
anti-ß-actin
1 2 3 4
1.00 1.10 1.31 1.36
c
PTEN
- +
R1881 (1 nM)
anti-FLIP
anti-PSA
anti-PTEN
anti-ß-actin
1 2
0.20 1.00
d
Fold change
1.2
0.8
0.4
0
**
**
*
*
- + - + - +
R1881
pCMV
FOXO3a TM
PTEN

Figure 7

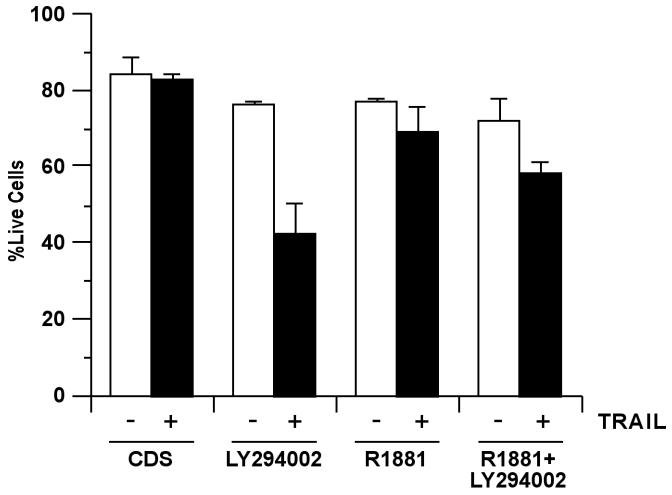
100
80
60
40
20
0
%Live Cells
- + - + - + - +
TRAIL
CDS
LY294002
R1881
R1881+
LY294002

Figure 8

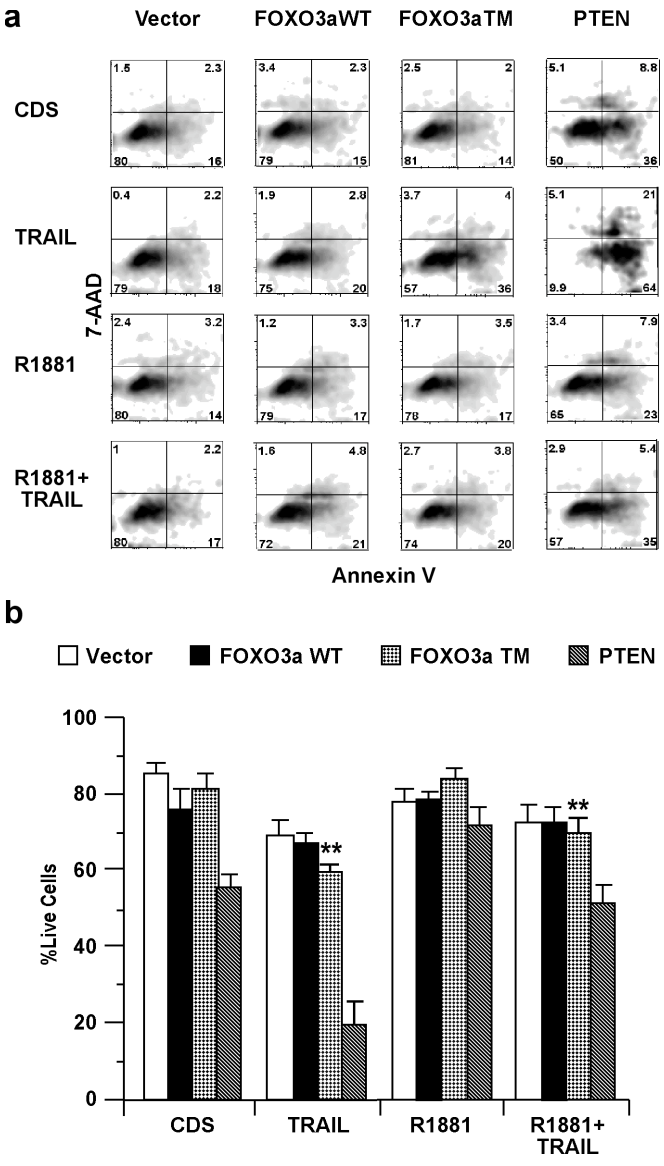
a
Vector
FOXO3aWT
FOXO3aTM
PTEN
CDS
TRAIL
R1881
R1881+ TRAIL
7-AAD
Annexin V
b
Vector
FOXO3a WT
FOXO3a TM
PTEN
%Live Cells
100
80
60
40
20
0
**
**
CDS
TRAIL
R1881
R1881+ TRAIL